

# The voltage-gated channels of $\text{Ca}^{2+}$ action potentials: Generalization

Chapter 4 explained the  $\text{Na}^+$ -dependent action potential propagated by axons. There are two other types of action potentials: (i) the  $\text{Na}^+/\text{Ca}^{2+}$ -dependent action potential present in axon terminals or heart muscle cells (**Figure 4.2d**), for example, where it is responsible for  $\text{Ca}^{2+}$  entry and an increase of intracellular  $\text{Ca}^{2+}$  concentration, a necessary prerequisite for neurotransmitter release (secretion) or muscle fibre contraction; and (ii) the  $\text{Ca}^{2+}$ -dependent action potential (in which  $\text{Na}^+$  ions do not participate) in dendrites of Purkinje cells of the cerebellum (see **Figure 17.9**) and in endocrine cells (**Figure 5.1a**). In Purkinje cell dendrites, it depolarizes the membrane and thus modulates neuronal integration; in endocrine cells it provides a  $\text{Ca}^{2+}$  entry to trigger hormone secretion.

## 5.1 PROPERTIES OF $\text{Ca}^{2+}$ -DEPENDENT ACTION POTENTIALS

In some neuronal cell bodies, in heart ventricular muscle cells and in axon terminals, the action potentials have a longer duration than  $\text{Na}^+$  spikes, with a plateau following the initial peak: these are the  $\text{Na}^+/\text{Ca}^{2+}$ -dependent action potentials (see **Figure 4.2b–d**). In some neuronal dendrites and some endocrine cells, action potentials have a small amplitude and a long duration: these are the  $\text{Ca}^{2+}$ -dependent action potentials (**Figure 5.1**). All action potentials are initiated in response to a membrane depolarization.  $\text{Na}^+$ ,  $\text{Na}^+/\text{Ca}^{2+}$  and  $\text{Ca}^{2+}$ -dependent action potentials differ in the type of voltage-gated channels responsible for their depolarization and repolarization phases. We

will examine the properties of a  $\text{Ca}^{2+}$ -dependent action potential.

### 5.1.1 $\text{Ca}^{2+}$ and $\text{K}^+$ ions participate in the action potential of endocrine cells

The activity of pituitary endocrine cells that release growth hormone is recorded in the perforated whole-cell configuration (current clamp mode; see Appendix 4.1). They display a spontaneous activity. When these cells are previously loaded with the  $\text{Ca}^{2+}$ -sensitive dye Fura-2, changes of intracellular  $\text{Ca}^{2+}$  concentration can be also quantified (see **Appendix 5.1**). Simultaneous recording of potential and  $[\text{Ca}^{2+}]_i$  changes shows that for each action potential there is a corresponding  $[\text{Ca}^{2+}]_i$  increase (**Figure 5.1a**). This strongly suggests that  $\text{Ca}^{2+}$  ions are entering the cell during action potentials.

*$\text{Ca}^{2+}$  ions participate in the depolarization phase of the action potential*

When the extracellular solution is changed from control Krebs to a  $\text{Ca}^{2+}$ -free solution, or when nifedipin, an L-type  $\text{Ca}^{2+}$  channel blocker, is added to the external medium (**Figure 5.1b**), the amplitude and risetime of the depolarization phase of the action potential gradually and rapidly decreases until action potentials are no longer evoked.

*$\text{K}^+$  ions participate in the repolarization phase of the action potential*

Application of charybdotoxin (CTX) or apamin, blockers of  $\text{Ca}^{2+}$ -activated  $\text{K}^+$  channels, increases the

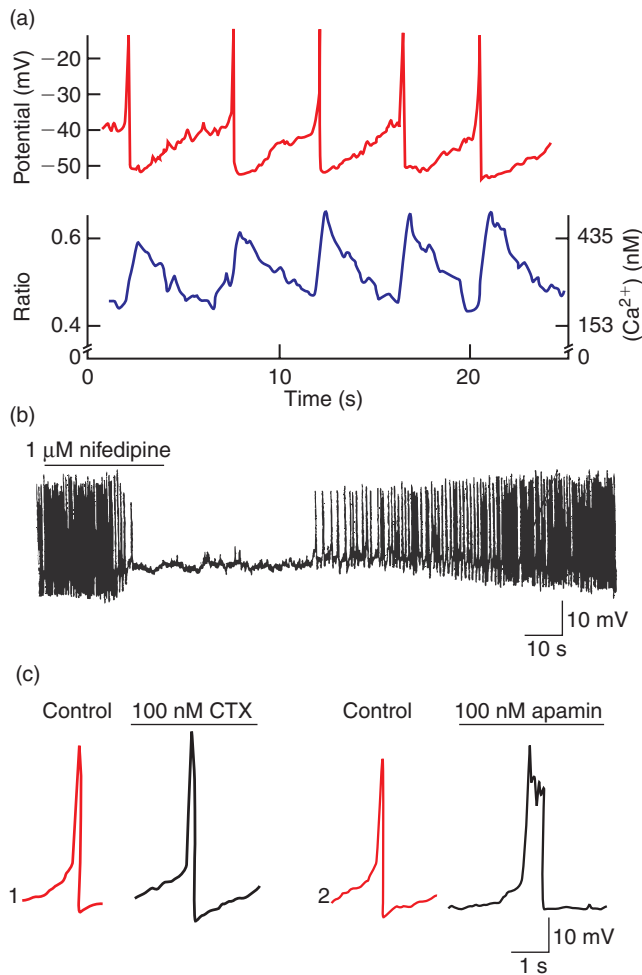


**FIGURE 5.1** The  $\text{Ca}^{2+}$ -dependent action potential of an endocrine cell.

Growth-hormone secreting cells of the anterior pituitary in culture are loaded with the  $\text{Ca}^{2+}$ -sensitive dye Fura-2 and their activity is recorded in perforated whole-cell patch configuration (current clamp mode). (a) Simultaneous recordings of action potentials (top trace) and cytosolic  $[\text{Ca}^{2+}]$  oscillations (bottom trace) in control conditions. (b) Nifedipin, an L-type  $\text{Ca}^{2+}$  channel blocker, is applied for 20 s. (c) Action potential in the absence and presence of blockers of  $\text{Ca}^{2+}$ -activated  $\text{K}^{+}$  channels, charybdotoxin (CTX, 1) and apamin (2). Adapted from Kwicic R, Robert C, Cannon R *et al.* (1998) Endogenous pacemaker activity of rat tumour somatotrophs. *J. Physiol.* 508, 883–905, with permission.

peak amplitude and prolongs the duration of action potentials (Figure 5.1c). Note that apamin also blocks the after-spike hyperpolarization (Figure 5.1c, right).

### 5.1.2 Questions about the $\text{Ca}^{2+}$ -dependent action potential

- What are the structural and functional properties of the  $\text{Ca}^{2+}$  and  $\text{K}^{+}$  channels involved? (Sections 5.2 and 5.3)?

- What represents the threshold potential for  $\text{Ca}^{2+}$ -dependent action potential initiation? Where are  $\text{Ca}^{2+}$ -dependent action potentials initiated? (Section 5.4)

## 5.2 THE TRANSIENT ENTRY OF $\text{Ca}^{2+}$ IONS THROUGH VOLTAGE-GATED $\text{Ca}^{2+}$ CHANNELS IS RESPONSIBLE FOR THE DEPOLARIZING PHASE OR THE PLATEAU PHASE OF $\text{Ca}^{2+}$ -DEPENDENT ACTION POTENTIALS

The voltage-gated  $\text{Ca}^{2+}$  channels involved in these action potentials are high threshold-activated (HVA)  $\text{Ca}^{2+}$  channels. There are three main types of such channels: the L-type (L for long lasting), the N-type (N for neuronal or for neither L nor T) and the P-type (P for Purkinje cells where they have been first described).

### 5.2.1 The voltage-gated $\text{Ca}^{2+}$ channels are a diverse group of multisubunit proteins

They are composed of a pore-forming  $\alpha_1$ -subunit of about 2000 amino acid residues (190–250 kDa), with an amino acid sequence and a predicted transmembrane structure like the previously characterized pore forming  $\alpha$ -subunit of  $\text{Na}^{+}$  channels: four repeated domains (I to IV), each of which contains six transmembrane segments (1 to 6) and a membrane-associated loop between transmembrane segments S5 and S6 of each domain (Figure 5.2a). It incorporates the conduction pore, the voltage sensor and gating apparatus and the known sites of channel regulation by second messengers, drugs and toxins. Auxiliary subunits can include a transmembrane disulphide-linked complex of  $\alpha_2$  and  $\delta$ -subunits, a  $\beta$ -subunit and in some cases a transmembrane  $\gamma$ -subunit. The  $\beta$ -subunit has predicted  $\alpha$ -helices but no transmembrane segments and is thought to be intracellular. They play a role in the expression and gating properties of the  $\text{Ca}^{2+}$  channels by modulating various properties of the  $\alpha_1$ -subunit.

The pharmacological and electrophysiological diversity of  $\text{Ca}^{2+}$  channels primarily arises from the diversity of  $\alpha_1$ -subunits. The primary structure of the different  $\alpha_1$ -subunits has been defined by homology screening and their function characterized by expression in mammalian cells or *Xenopus* oocytes. The recent nomenclature divides the  $\text{Ca}^{2+}$  channels in three structurally and functionally related families ( $\text{Ca}_v1$ ,  $\text{Ca}_v2$ ,  $\text{Ca}_v3$ ) to indicate the principal permeating ion (Ca) and the principal physiological regulator (v for voltage), followed by a number that indicates the gene subfamily

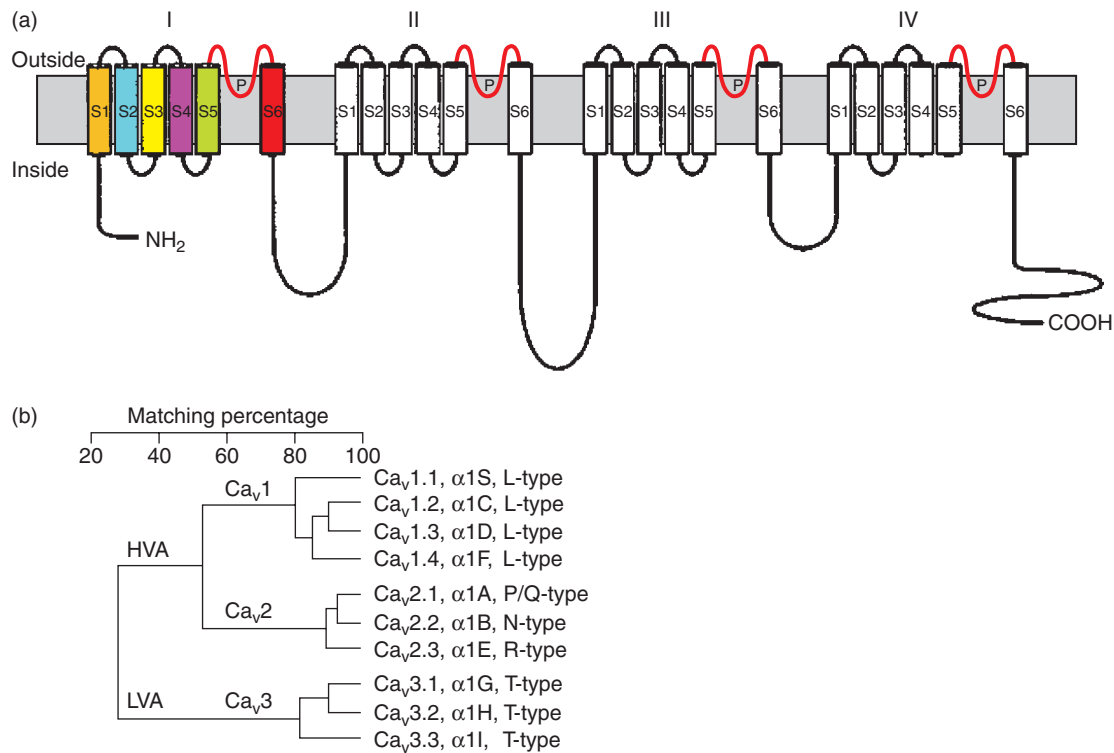


**FIGURE 5.2** Subunits of voltage-gated  $\text{Ca}^{2+}$  channels.

(a) Membrane topology for the  $\alpha_1$ -subunit of a cardiac L-type  $\text{Ca}^{2+}$  channel (P: the P loops). (b) Evolutionary tree of voltage-gated  $\alpha_1$ -subunit of  $\text{Ca}^{2+}$  channels. Low voltage-activated  $\text{Ca}^{2+}$  channels (LVA) appear to have diverged from an ancestral  $\text{Ca}^{2+}$  channel before the bifurcation of the high voltage-activated (HVA) channels in Ca<sub>v</sub>1 and Ca<sub>v</sub>2 subfamilies. (a) Adapted from Sather WA (2003) Permeation and selectivity in calcium channels. *Annu. Rev. Physiol.* 65, 133–159. (b) Adapted from Perez-Reyes E, Cribbs LL, Daud A *et al.* (1998) Molecular characterization of a neuronal low voltage-activated T-type calcium channel. *Nature* 391, 896–900.

(1, 2 or 3). The number following the decimal point identifies the specific channel isoform (e.g. Ca<sub>v</sub>1.1) (Figure 5.2b). High-threshold  $\text{Ca}^{2+}$  channels comprise L (Ca<sub>v</sub>1), P/Q (Ca<sub>v</sub>2.1), N (Ca<sub>v</sub>2.2) and R (Ca<sub>v</sub>2.3)-type  $\text{Ca}^{2+}$  channels.

### How to record the activity of $\text{Ca}^{2+}$ channels in isolation

This needs to block the voltage-gated channels that are not permeable to  $\text{Ca}^{2+}$  ions. Different strategies can be used: in whole-cell or intracellular recordings, TTX and TEA are added to the extracellular solution and K<sup>+</sup> ions are replaced by Cs<sup>+</sup> in the intrapipette solution, in order to block voltage-gated Na<sup>+</sup> and K<sup>+</sup> channels. In cell-attached recordings the patch pipette is filled with a solution containing  $\text{Ca}^{2+}$  or  $\text{Ba}^{2+}$  ions as the charge carrier. When  $\text{Ba}^{2+}$  substitutes for  $\text{Ca}^{2+}$  in the extracellular solution, the inward currents recorded in response to a depolarizing step are  $\text{Ba}^{2+}$  currents.  $\text{Ba}^{2+}$  is often preferred to  $\text{Ca}^{2+}$  since it carries current twice as effectively as  $\text{Ca}^{2+}$  and poorly inactivates  $\text{Ca}^{2+}$  channels

(see Section 5.2.3). As a consequence, unitary  $\text{Ba}^{2+}$  currents are larger than  $\text{Ca}^{2+}$  ones and can be studied more easily.

Another challenge is to separate the various types of  $\text{Ca}^{2+}$  channels in order to record the activity of only one type (since in most of the cells they are co-expressed). These different  $\text{Ca}^{2+}$  channels are the high voltage-activated L, N and P channels (this chapter) and the low-threshold T channel. T-type  $\text{Ca}^{2+}$  channels are low threshold-activated channels, also called subliminal  $\text{Ca}^{2+}$  channels, that can be identified by their low threshold of activation and their rapid inactivation. They are studied with other subliminal channels in Section 14.2.2.

HVA  $\text{Ca}^{2+}$  channels exhibit overlapping electrophysiological profiles. It is important to separate them in order to study their characteristics and to identify their respective roles in synaptic integration (dendritic  $\text{Ca}^{2+}$  channels), in transmitter release ( $\text{Ca}^{2+}$  channels of axon terminals), hormone secretion ( $\text{Ca}^{2+}$  channels of endocrine cells), muscle contraction ( $\text{Ca}^{2+}$  channels of smooth, skeletal or cardiac muscle cells).

HVA  $\text{Ca}^{2+}$  channels can be separated by using  $\text{Ca}^{2+}$  channel blockers, which can be subdivided in three general classes: small organic blockers; peptide toxins; and inorganic blockers. Small organic blockers include the dihydropyridines (DHP) that selectively block L-type channels (these channels are also selectively opened by Bay K 8644). Peptide toxins include an  $\omega$ -conotoxin of the marine snail *Conus geographicus* that selectively blocks N-type channels and a purified polyamine fraction of the funnel-web spider (*Agelenopsis aperta*) venom (FTX) or a peptide component of the same venom,  $\omega$ -agatoxin IVA ( $\omega$ -Aga-IVA) that selectively block P-type channels. Inorganic blockers include divalent or trivalent metal ions such as cadmium, nickel, but they are not selective and are thus not used to separate the different types of HVA channels.

### 5.2.2 The L, N and P-type $\text{Ca}^{2+}$ channels open at membrane potentials positive to $-20$ mV; they are high-threshold $\text{Ca}^{2+}$ channels

*The L-type  $\text{Ca}^{2+}$  channel has a large conductance and inactivates very slowly with depolarization*

The activity of single L-type  $\text{Ca}^{2+}$  channels is recorded in sensory neurons of the chick dorsal root ganglion in patch clamp (cell-attached patch with  $\text{Ba}^{2+}$  as the charge carrier). In response to a test depolarization to  $+20$  mV from a *depolarized* holding potential ( $-40$  to  $0$  mV), unitary inward  $\text{Ba}^{2+}$  currents are evoked and recorded throughout the duration of the depolarizing step (Figure 5.3a).

The voltage-dependence of activation is studied with depolarizations to various test potentials from a holding potential of  $-40$  mV (Figure 5.4). With test depolarizations up to  $+10$  mV, openings are rare and of short duration. Activation of the channel becomes significant at  $+10$  mV: openings are more frequent and of longer duration. At all potentials tested, openings are distributed relatively evenly throughout the duration of the depolarizing step (Figures 5.3a and 5.4a). At  $-20$  mV, the mean single-channel amplitude of the L current ( $i_L$ ) is around  $-2$  pA.  $i_L$  amplitude diminishes linearly with depolarization: the  $i_L/V$  relation is linear between  $-20$  and  $+20$  mV. Between these membrane potentials, the unitary conductance,  $\gamma_L$ , is constant and equal to  $20$ – $25$  pS in  $110$  mM  $\text{Ba}^{2+}$  (Figure 5.4c).

The main characteristics of L-type channels are (i) their very slow inactivation during a depolarizing step; (ii) their sensitivity to dihydropyridines; and (iii) their loss of activity in excised patches. Bay K 8644 is a dihydropyridine compound that increases dramatically the mean open time of an L-type channel without

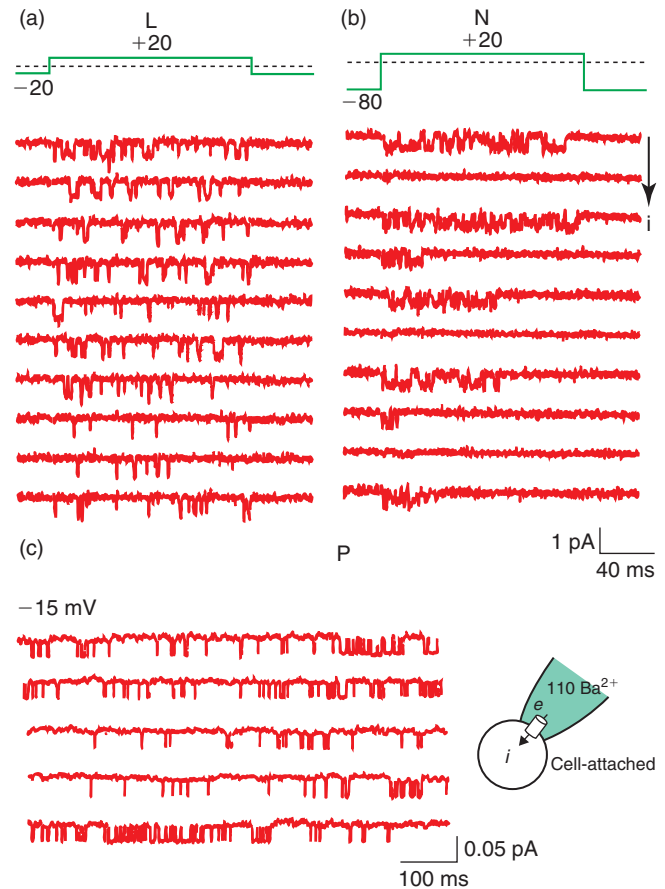


**FIGURE 5.3** Single-channel recordings of the high-threshold  $\text{Ca}^{2+}$  channels: the L, N and P channels.

The activity of (a) single L and (b) N  $\text{Ca}^{2+}$  channels is recorded in patch clamp (cell-attached patches) from dorsal root ganglion cells and that of a single P channel (c) is recorded from a lipid bilayer in which a P channel isolated from cerebellum has been incorporated. All recordings are performed with  $\text{Ba}^{2+}$  (110 or 80 mM) as the charge carrier. In response to a test depolarizing step to  $+20$  mV (a, b) or at a depolarized holding potential of  $-15$  mV (c), unitary inward currents are recorded. Upper traces are voltage and the corresponding unitary current traces are the bottom traces (5–10 trials).  $V_H = -20$  mV in (a),  $-80$  mV in (b) and  $-15$  mV in (c). In (a) and (b) the intrapipette solution contains: 110 mM  $\text{BaCl}_2$ , 10 mM HEPES and  $200 \mu\text{M}$  TTX. The extracellular solution bathing the membrane outside the patch contains (in mM): 140 K aspartate, 10 K-EGTA, 10 HEPES, 1  $\text{MgCl}_2$  in order to zero the cell resting membrane potential. In (c) the solution bathing the extracellular side of the bilayer contains (in mM): 80  $\text{BaCl}_2$ , 10 HEPES. The solution bathing the intracellular side of the bilayer in (c) contains (in mM): 120 CsCl, 1  $\text{MgCl}_2$ , 10 HEPES. Parts (a) and (b) adapted from Nowycky MC, Fox AP, Tsien RW (1985) Three types of neuronal calcium channel with different calcium agonist sensitivity. *Nature* **316**, 440–443, with permission. Part (c) adapted from Llinas R, Sugimori M, Lin JW, Cherksey B (1989) Blocking and isolation of a calcium channel from neurons in mammals and cephalopods utilizing a toxin fraction (FTX) from funnel web spider poison. *Proc. Natl Acad. Sci. USA* **86**, 1689–1693, with permission.

changing its unitary conductance (Figure 5.5). It has no effect on the other  $\text{Ca}^{2+}$  channel types (see Figure 5.9). Bay K 8644 binds to a specific site on the  $\alpha_1$ -subunit of L channels and changes the gating mode from brief

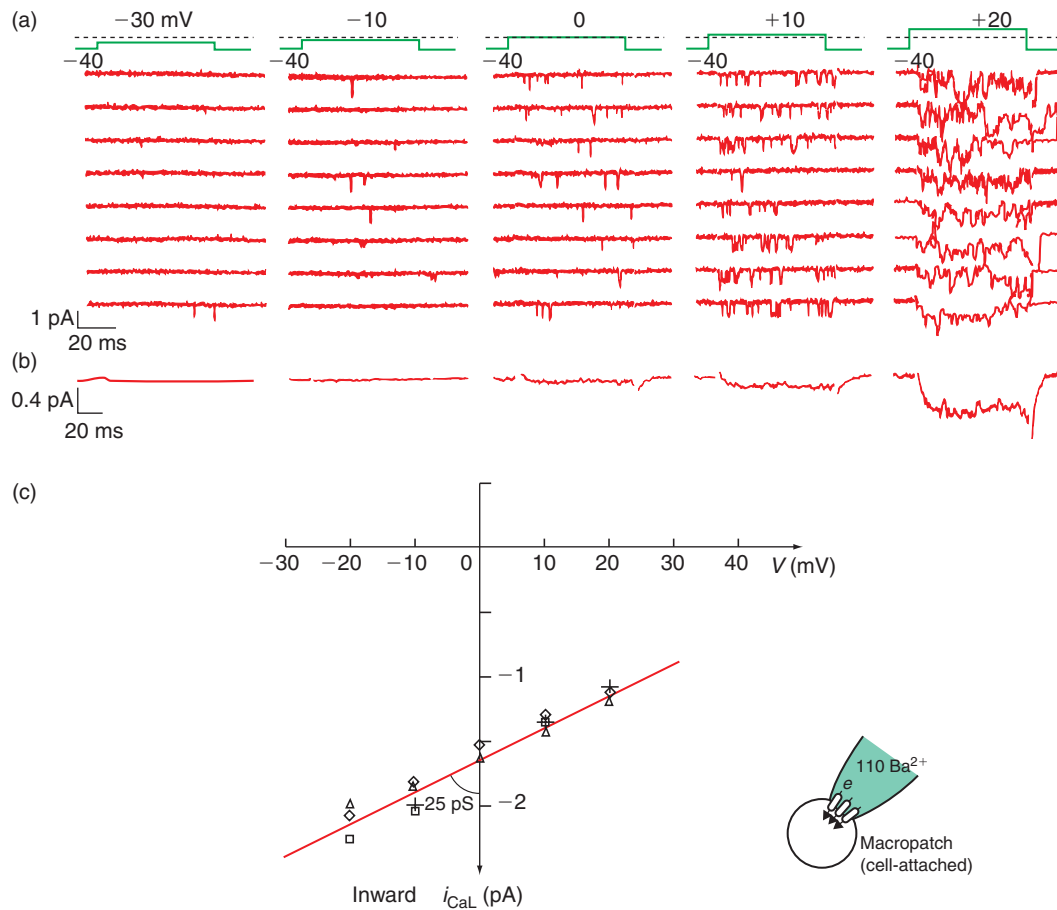


**FIGURE 5.4 Voltage dependence of the unitary L-type  $\text{Ca}^{2+}$  current.**

(a) The activity of L channels (the patch of membrane contains more than one L channel) is recorded in patch clamp (cell-attached patch) in a sensory dorsal root ganglion neuron. The patch is depolarized to  $-30$ ,  $-10$ ,  $0$ ,  $+10$  and  $+20$  mV from a holding potential of  $-40$  mV. (b) Macroscopic current traces obtained by averaging at least 80 corresponding unitary current recordings such as those in (a). The probability of the L channels being in the open state increases with the test depolarization so that at  $+20$  mV, openings of the 4–5 channels present in the patch overlap, leading to a sudden increase in the corresponding macroscopic current. (c) The unitary L current amplitude ( $i_L$ ) is plotted against membrane potential (from  $-20$  to  $+20$  mV) in the absence (+, square) or presence ( $\Delta$ , lozange) of Bay K 8644 in the patch pipette. The amplitude of  $i_L$  decreases linearly with depolarization between  $-20$  and  $+20$  mV with a slope  $\gamma_L = 25$  pS. The intrapipette solution contains (in mM): 110 BaCl<sub>2</sub>, 10 HEPES. The extracellular solution bathing the extracellular side of the membrane outside of the recording pipette contains (in mM): 140 K-aspartate, 10 K-EGTA, 1 MgCl<sub>2</sub>, 10 HEPES. A symmetric K<sup>+</sup> solution is applied in order to zero the cell resting potential. Adapted from Fox AF, Nowycky MC, Tsien RW (1987) Single-channel recordings of three types of calcium channels in chick sensory neurons. *J. Physiol.* 394, 173–200, with permission.

openings to long-lasting openings even at weakly depolarized potentials ( $V_{\text{step}} = -30$  mV). Other dihydropyridine derivatives such as nifedipine, nimodipine and nitrendipine selectively block L channels (see **Figure 5.16**).

The loss of activity of an L channel in excised patch can be observed in outside-out patches. In response to a test depolarization to  $+10$  mV the activity of an L channel rapidly disappears (**Figure 5.6**). To determine the nature of the cytoplasmic constituent(s) necessary to restore the activity of the L channel, inside-out patches are performed, a configuration that allows a

change of the medium bathing the intracellular side of the membrane.

The activity of a single L channel is first recorded in cell-attached configuration in response to a test depolarization to  $0$  mV (**Figure 5.7**). Then the membrane is pulled out in order to obtain an inside-out patch. The L-type activity rapidly disappears and is not restored by adding ATP–Mg to the intracellular solution. In contrast, when the catalytic subunit of the cAMP-dependent protein kinase (PKA) is added, the L-channel activity reappears (the catalytic subunit of PKA does not need the presence of cAMP to be active). This suggests that PKA directly

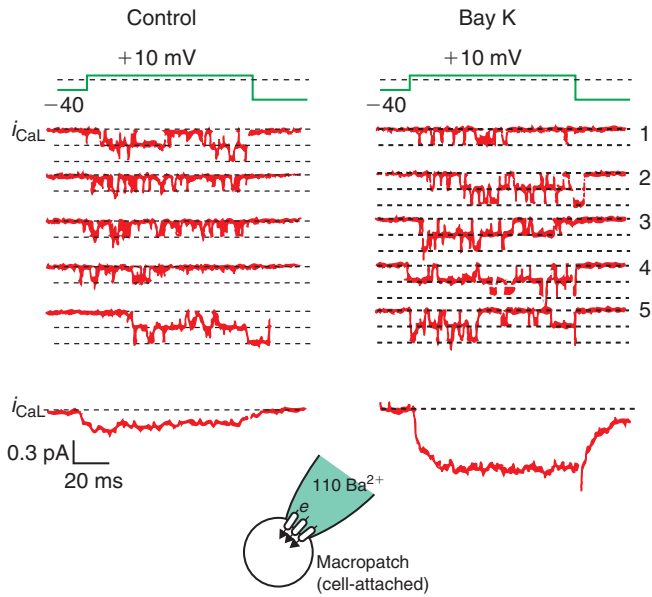


**FIGURE 5.5** Bay K 8644 promotes long-lasting openings of L-type  $\text{Ca}^{2+}$  channels.

The activity of three L channels is recorded in patch clamp (cell-attached patch). Top traces: a depolarizing step to +10 mV from a holding potential of -40 mV is applied at a low frequency. Middle traces (1 to 5): five consecutive unitary current traces recorded in the absence (left) and presence (right) of  $5 \mu\text{M}$  Bay K 8644 in the bathing solution. Recordings are obtained from the same cell. Dashed line indicates the mean amplitude of the unitary current (-1.28 pA) which is unchanged in the presence of Bay K. Bottom traces: macroscopic current traces obtained by averaging at least 80 corresponding unitary current recordings. Adapted from Fox AP, Nowycky MC, Tsien RW (1987) Single-channel recordings of three types of calcium channels in chick sensory neurones. *J. Physiol.* 394, 173–200, with permission.

phosphorylates the L channel thus allowing its activation by the depolarization. It means that, in physiological conditions, the activity of L channels requires the activation of the following cascade: the activation of adenylate cyclase by the  $\alpha$ -subunit of the G protein, the formation of cAMP and the subsequent activation of protein kinase A. Other kinases might also play a role. That is how neurotransmitters and a wide variety of hormones modulate L-type  $\text{Ca}^{2+}$  currents in neurons but also in endocrine cells and in smooth, skeletal and cardiac muscle.

*The N-type  $\text{Ca}^{2+}$  channel inactivates with depolarization in the tens of milliseconds range and has a smaller unitary conductance than the L-type channel*

The activity of single N-type channels is recorded in the same preparation in patch clamp (cell-attached patch, with  $\text{Ba}^{2+}$  as the charge carrier). In contrast to the L channels, N channels inactivate with depolarization. Therefore their activity has to be recorded in response to a test depolarization from a hyperpolarized holding potential (-80 to -60 mV) (Figure 5.3b). At holding potentials positive to -40 mV (e.g. -20 mV; Figure 5.3a), the N channel(s) is inactivated and its activity is absent in the recordings.

N-channel activity differs from that of the L channel in several aspects:

- N channels often open in bursts and inactivate with time and voltage (see Section 5.2.3).

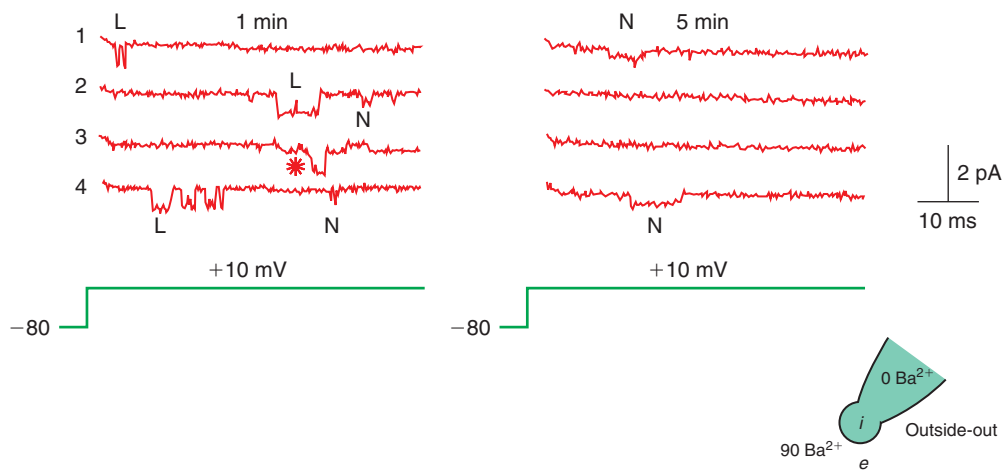


**FIGURE 5.6** In excised patches, the activity of L channels disappears within minutes.

The activity of an L and N channel is recorded in patch clamp (outside-out patches from a pituitary cell line in culture) in response to a depolarizing pulse to +10 mV from a holding potential of -80 mV. Left: One minute after forming the excised patch, the two types of channels open one at a time or their openings overlap (line 3, \*). Five minutes after, only the activity of the N-type is still present. The activity of the L-type will not reappear spontaneously. The extracellular solution contains (in mM): 90  $\text{BaCl}_2$ , 15 TEACl,  $2 \times 10^{-3}$  TTX, 10 HEPES. The intrapipette solution contains (in mM): 120 CsCl, 40 HEPES. Adapted from Armstrong D and Eckert R (1987) Voltage-activated calcium channels that must be phosphorylated to respond to membrane depolarization. *Proc. Natl Acad. Sci. USA* 84, 2518–2522, with permission.

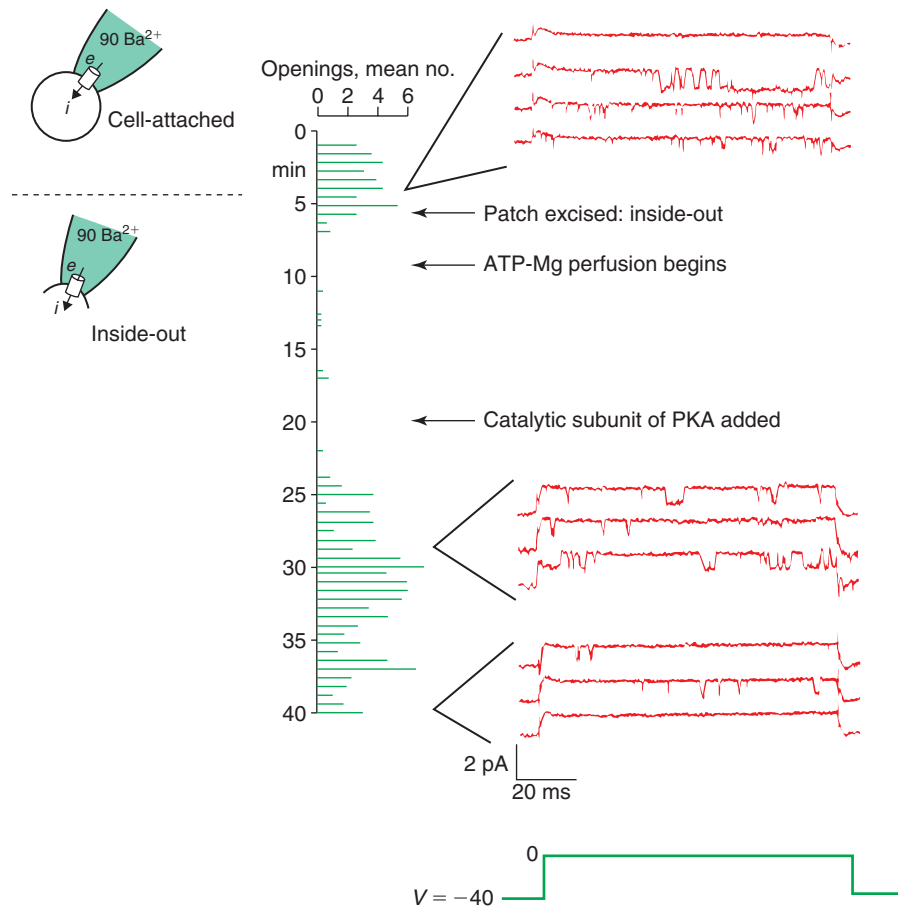


**FIGURE 5.7 Phosphorylation reverses the loss of activity of the L channels in an inside-out patch.** The activity of an L-type channel is recorded in patch clamp (inside-out patch from a pituitary cell line in culture) in response to a depolarizing pulse to 0 mV from a holding potential of  $-40$  mV. The horizontal traces are the unitary current traces and the vertical histogram represents the average number of channel openings per trace, determined over 30 s intervals and plotted versus time of the experiment (0–40 min). After 5 min of recording in the cell-attached configuration, the activity of the channel is recorded in the inside-out configuration. See text for further explanations. The intrapipette solution contains (in mM): 90  $\text{BaCl}_2$ , 15 TEACl,  $2 \times 10^{-3}$  TTX, 10 HEPES. The solution bathing the intracellular side of the patch contains (in mM): 120 CsCl, 40 HEPES. From Armstrong D and Eckert R (1987) Voltage-activated calcium channels that must be phosphorylated to respond to membrane depolarization. *Proc. Natl Acad. Sci. USA* **84**, 2518–2522, with permission.

- Measured at the same test potential, the mean amplitude of the N unitary current is smaller than that of L (e.g.  $i_N = -1.22 \pm 0.03$  pA and  $i_L = -2.07 \pm 0.09$  at  $-20$  mV; **Figure 5.3a, b**) which makes its mean unitary conductance also smaller ( $\gamma_N = 13$  pS in 110 mM  $\text{Ba}^{2+}$ ; **Figure 5.8b**).
- N channels are insensitive to dihydropyridines but are selectively blocked by  $\omega$ -conotoxin GVIA.
- N channels do not need to be phosphorylated to open (**Figure 5.6**).

*The P-type  $\text{Ca}^{2+}$  channel differs from the N channel by its pharmacology*

The activity of a single P-type channel is recorded from lipid bilayers in which purified P channels from

cerebellar Purkinje cells have been incorporated.  $\text{Ba}^{2+}$  ions are used as the charge carrier. The activity of the P channel is recorded at different steady holding potentials. At  $-15$  mV, the channel opens, closes and reopens during the entire depolarization, showing little time-dependent inactivation (**Figure 5.3c**). The mean unitary conductance,  $\gamma_P$ , is 10–15 pS in 80 mM  $\text{Ba}^{2+}$ . Recordings performed in dendrites or the soma of cerebellar Purkinje cells with patch clamp techniques (cell-attached patches) gave similar values of the unitary conductance ( $\gamma_P = 9$ –19 pS in 110 mM  $\text{Ba}^{2+}$ ), but for undetermined reasons the threshold for activation is at a more depolarized potential ( $-15$  mV) than for isolated P channels inserted in lipid bilayers ( $-45$  mV). When the funnel web toxin fraction (FTX) is added to the recording patch pipette (the intrapipette solution bathes the extracellular

side of the patch), only rare high-threshold unitary currents are recorded from Purkinje cell dendrites or soma at all potentials tested (Bay K 8644 or  $\omega$ -conotoxin have no effect). These results suggest that the P channel is the predominant high-threshold  $\text{Ca}^{2+}$  channel expressed by Purkinje cells. They also show that the use of selective toxins allows the differentiation between P, N and L channels.

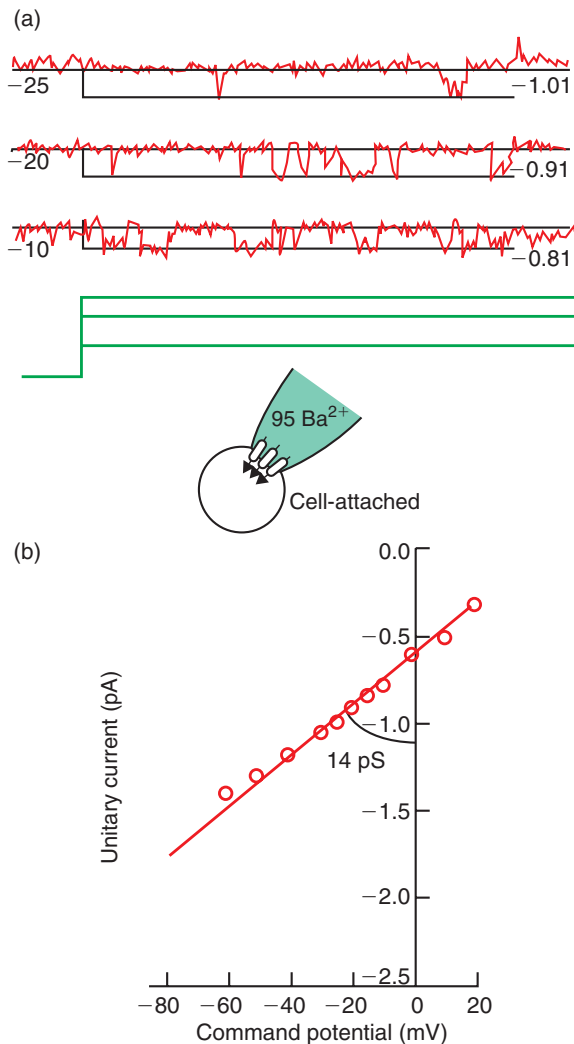


**FIGURE 5.8** Voltage dependence of the unitary N current,  $i_N$ . (a) The activity of an N channel is recorded in patch clamp (cell-attached patch) in a granule cell of the hippocampus. The patch is depolarized to  $-25$ ,  $-20$  and  $-10$  mV from a holding potential of  $-80$  mV. The amplitude of the unitary current at these voltages is indicated at the end of each recording. (b) The unitary N current amplitude ( $i_N$ ) is plotted against membrane potential (from  $-60$  to  $+20$  mV). The amplitude of  $i_N$  decreases linearly with depolarization between  $-60$  and  $+20$  mV with a slope  $\gamma_N = 14$  pS ( $n = 14$  patches). Adapted from Fisher RE, Gray R, Johnston D (1990) Properties and distribution of single voltage-gated calcium channels in adult hippocampal neurons. *J. Neurophysiol.* **64**, 91–104, with permission.

### 5.2.3 Macroscopic L, N and P-type $\text{Ca}^{2+}$ currents activate at a high threshold and inactivate with different time courses

The macroscopic L, N and P-type  $\text{Ca}^{2+}$  currents ( $I_{\text{Ca}}$ ), at time  $t$  during a depolarizing voltage step, are equal to:  $I_{\text{Ca}} = Np_t i_{\text{Ca}}$  where  $N$  is the number of L, N or P channels in the membrane,  $p_t$  is their probability of being open at time  $t$  during the depolarizing step,  $Np_t$  is the number of open channels at time  $t$  during the depolarizing step and  $i_{\text{Ca}}$  is the unitary L, N or P current. At steady state,  $I_{\text{Ca}} = Np_o i_{\text{Ca}}$ , where  $p_o$  is the probability of the channel being open at steady state.

*The I/V relations for L, N and P-type  $\text{Ca}^{2+}$  currents have a bell shape with a peak amplitude at positive potentials*

The I/V relation of the different types of high threshold  $\text{Ca}^{2+}$  currents is studied in whole-cell recordings in the presence of external  $\text{Ca}^{2+}$  as the charge carrier. To separate the L, N and P currents, specific blockers are added to the external medium or the membrane potential is clamped at different holding potentials. With this last procedure, the L current can be separated from other  $\text{Ca}^{2+}$  currents since it can be evoked from depolarized holding potentials. As shown in **Figure 5.9**, the L and N currents averaged from the corresponding unitary currents recorded in  $110$  mM  $\text{Ba}^{2+}$  clearly differ in their time course. The averaged N current decays to zero level in  $40$  ms while the averaged L current remains constant during the  $120$  ms depolarizing step to  $+10$  mV. As already observed (**Figures 5.3a, b**), by

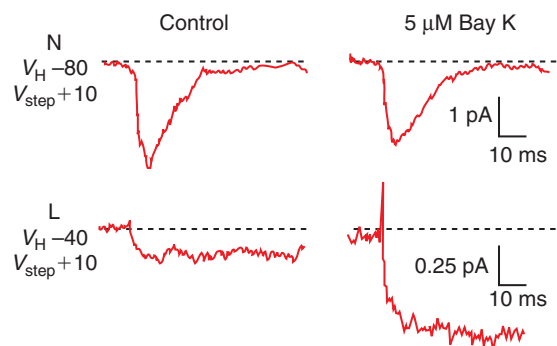


**FIGURE 5.9** Averaged N- and L-type  $\text{Ca}^{2+}$  currents. Single-channel N current averages (top traces) and L current averages (bottom traces) from cell-attached recordings of dorsal root ganglion cells with  $\text{Ba}^{2+}$  as the charge carrier (see also Figure 5.3a,b). Currents are averaged before (left) and after (right) exposure to  $5 \mu\text{M}$  Bay K 8644. Voltage steps from  $-80$  mV to  $+10$  mV (top traces) and from  $-40$  to  $+10$  mV (bottom traces). From Nowycky MC, Fox AP, Tsien RW (1985) Three types of neuronal calcium channel with different calcium agonist sensitivity. *Nature* **316**, 440–443, with permission.

holding the membrane at a depolarized potential, the N current inactivates and the L current can be studied in isolation.

The macroscopic N- and L-type  $\text{Ca}^{2+}$  currents are studied in spinal motoneurons of the chick in patch clamp (whole-cell patch) in the presence of  $\text{Na}^+$  and  $\text{K}^+$  channel blockers and in the presence of a T-type  $\text{Ca}^{2+}$  channel blocker. In response to a depolarizing voltage step to +20 mV from a holding potential of -80 mV, a mixed N and L whole-cell current is recorded (Figure 5.10a). When the holding potential is depolarized to 0 mV, a voltage step to +20 mV now only evokes the L current

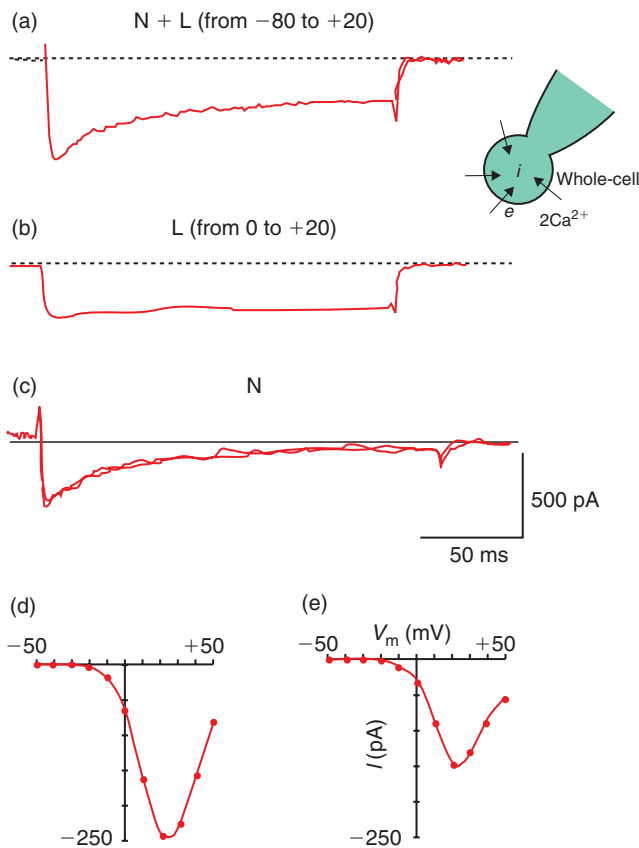


**FIGURE 5.10** N- and L-type macroscopic  $\text{Ca}^{2+}$  currents.

(a) The mixed N and L macroscopic current is recorded with  $\text{Ca}^{2+}$  as the charge carrier (whole-cell patch) from chick limb motoneurons in culture in response to a voltage step from -80 to +20 mV. (b) The macroscopic L current is recorded in isolation by changing the holding potential to 0 mV. (c) The difference current obtained by subtracting the L current from the N and L current (a) is the N current. (d)  $I/V$  relation for the L current recorded as in (b). (e)  $I/V$  relation for the N current obtained as the difference current. The intrapipette solution contains (in mM): 140 Cs aspartate, 5  $\text{MgCl}_2$ , 10 Cs EGTA, 10 HEPES, 0.1  $\text{Li}_2\text{GTP}$ , 1  $\text{MgATP}$ . The bathing solution contains (in mM): 146  $\text{NaCl}$ , 2  $\text{CaCl}_2$ , 5  $\text{KCl}$ , 1  $\text{MgCl}_2$ , 10 HEPES. Adapted from McCobb DP, Best PM, Beam KG (1989) Development alters the expression of calcium currents in chick limb motoneurons. *Neuron* 2, 1633–1643, with permission.

(Figure 5.10b). The difference current obtained by subtracting the L current from the mixed N and L current gives the N current (Figure 5.10c). The  $I/V$  relations of these two  $\text{Ca}^{2+}$  currents have a bell shape with a peak around +20 mV (Figures 5.10d, e). For comparison the peak amplitude of the macroscopic  $\text{Na}^+$  current is around -40 mV (see Figure 4.12a).

The macroscopic P-type  $\text{Ca}^{2+}$  current is studied in cerebellar Purkinje cells. These neurons express T, P and few L-type  $\text{Ca}^{2+}$  channels. In the presence of  $\text{Na}^+$  and  $\text{K}^+$  channel blockers and by choosing a holding potential where the low threshold T current is inactivated, the macroscopic P current can be studied. The  $I_P/V$  relation has a bell shape. The maximal amplitude is recorded around -10 mV (Figure 5.11).

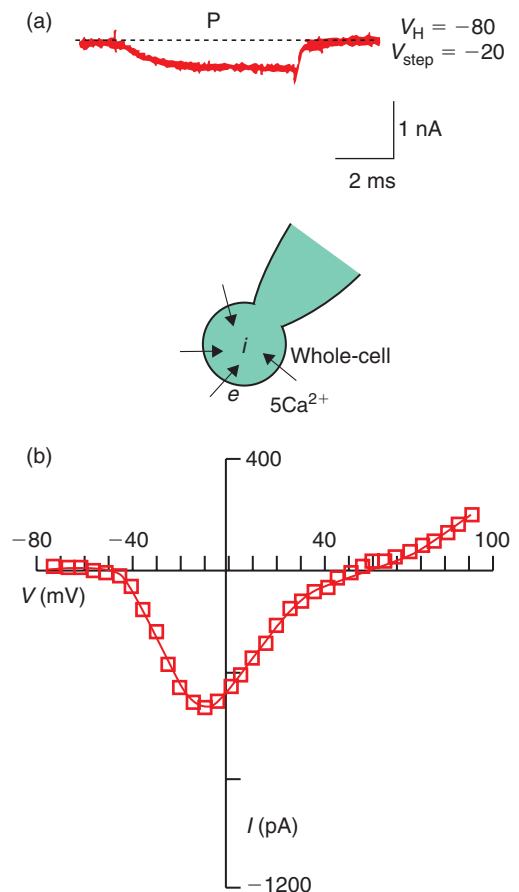


**FIGURE 5.11** P-type macroscopic  $\text{Ca}^{2+}$  current.

The whole-cell P current recorded from acutely dissociated Purkinje cells (whole-cell patch) with  $\text{Ca}^{2+}$  as the charge carrier. (a) Whole-cell P current recorded in response to a depolarizing pulse to -20 mV from a holding potential of -80 mV. (b)  $I/V$  relation of the P current. In the recordings the low threshold T-type  $\text{Ca}^{2+}$  current was either absent, inactivated or subtracted. The intrapipette solution contains (in mM): 120 TEA glutamate, 9 EGTA, 4.5  $\text{MgCl}_2$ , 9 HEPES. The bathing solution contains (in mM): 5  $\text{CaCl}_2$ , 154 TEACl, 0.2  $\text{MgCl}_2$ , 10 glucose, 10 HEPES. Adapted from Reagan LJ (1991) Voltage-dependent calcium currents in Purkinje cells from rat cerebellar vermis. *J. Neurosci.* 7, 2259–2269, with permission.

The bell shape of all the  $I_{\text{Ca}}/V$  relations is explained by the gating properties of the  $\text{Ca}^{2+}$  channels and the driving force for  $\text{Ca}^{2+}$  ions. The peak amplitude of  $I_{\text{Ca}}$  increases from the threshold potential to a maximal amplitude (Figures 5.10d,e, 5.11b and 5.12a) as a result of two opposite factors: the probability of opening which strongly increases with depolarization (Figure 5.12b) and the driving force for  $\text{Ca}^{2+}$  which linearly decreases with depolarization ( $i_{\text{Ca}}$  linearly diminishes). After a maximum, the peak amplitude of  $I_{\text{Ca}}$  decreases owing to the progressive decrease of the driving force for  $\text{Ca}^{2+}$  ions and the increase of the number of inactivated channels. Above +30/+40 mV, the probability of opening ( $p_o$ ) no longer plays a role since it is maximal (Figure 5.12b).  $I_{\text{Ca}}$  reverses polarity between +50 mV and +100 mV, depending on the preparation studied. This value is well below the theoretical  $E_{\text{Ca}}$ .

This discrepancy is partly due to the strong asymmetrical concentrations of  $\text{Ca}^{2+}$  ions. To measure the reversal potential of  $I_{\text{Ca}}$ , the outward current through  $\text{Ca}^{2+}$  channels must be measured. This outward current, caused by the extremely small intracellular concentration of  $\text{Ca}^{2+}$  ions, is carried by  $\text{Ca}^{2+}$  ions but also by internal  $\text{K}^+$  ions, which are around  $10^6$  times more concentrated than internal  $\text{Ca}^{2+}$  ions. This permeability

of  $\text{Ca}^{2+}$  channels to  $\text{K}^+$  ions ‘pulls down’ the reversal potential of  $I_{\text{Ca}}$  towards  $E_{\text{K}}$ .

### Activation–inactivation properties

Activation properties are analyzed by recording the macroscopic L, N or P currents in response to increasing test depolarizations from a fixed hyperpolarized holding potential (–80 mV, Figures 5.13b, 5.14b and 5.15b). In dorsal ganglion neurons, the L and N currents are half activated around 0 mV (Figures 5.13c and 5.14c) while in Purkinje cells the P current is half activated around –20 mV (Figure 5.15c).

### Voltage-gated $\text{Ca}^{2+}$ channels show varying degrees of inactivation

Inactivation properties are analyzed by recording the macroscopic L, N or P-type  $\text{Ca}^{2+}$  currents evoked by a voltage step to a fixed potential from various holding potentials (with  $\text{Ca}^{2+}$  as the charge carrier). The L current is half inactivated around –40 mV (Figures 5.13a, c), the N current around –60 mV (Figures 5.14a, c) and the P current around –45 mV (Figures 5.15a, c).

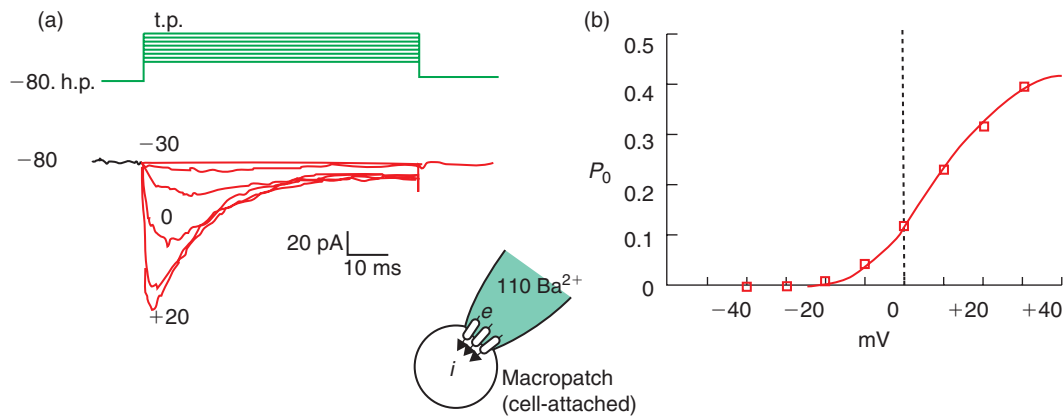


**FIGURE 5.12** The peak opening probability of the N current.

The macroscopic N current is recorded in a dorsal root ganglion neuron from a cell-attached patch containing hundreds of N channels (macropatch). (a) Current recordings (bottom traces) in response to test potentials (t.p.) ranging from –30 mV to +20 mV from a holding potential (h.p.) of –80 mV (upper traces). (b) Voltage-dependence of the peak opening probability ( $p_o$ ) from data obtained in (a). Values of  $p_o$  are obtained by dividing the peak current  $I$  by the unitary current  $i_{\text{N}}$  obtained at each test potential and by an estimate of the number of channels in the patch (599):  $p_o = I/Ni_{\text{N}}$ .  $N$  was determined by comparison with the single-channel experiment in Figure 5.3b, which shows that in response to a depolarization to +20 mV from a holding potential of –80 mV,  $p_o = 0.32$  and  $i_{\text{N}} = 0.76$  pA.  $I$ , the peak current evoked by the same voltage protocol, is 145 pA.  $N = I/p_o i_{\text{N}} = 145/(0.32 \times 0.76) = 599$  channels. The intrapipette solution contains (in mM): 100 CsCl, 10 Cs-EGTA, 5 MgCl<sub>2</sub>, 40 HEPES, 2 ATP, 0.25 cAMP; pH = 7.3. The extracellular solution contains (in mM): 10 CaCl<sub>2</sub>, 135 TEACl, 10 HEPES,  $0.2 \times 10^{-3}$  TTX; pH = 7.3. From Nowycky MC, Fox AP, Tsien RW (1985) Three types of neuronal calcium channel with different calcium agonist sensitivity. *Nature* 316, 440–443, with permission.

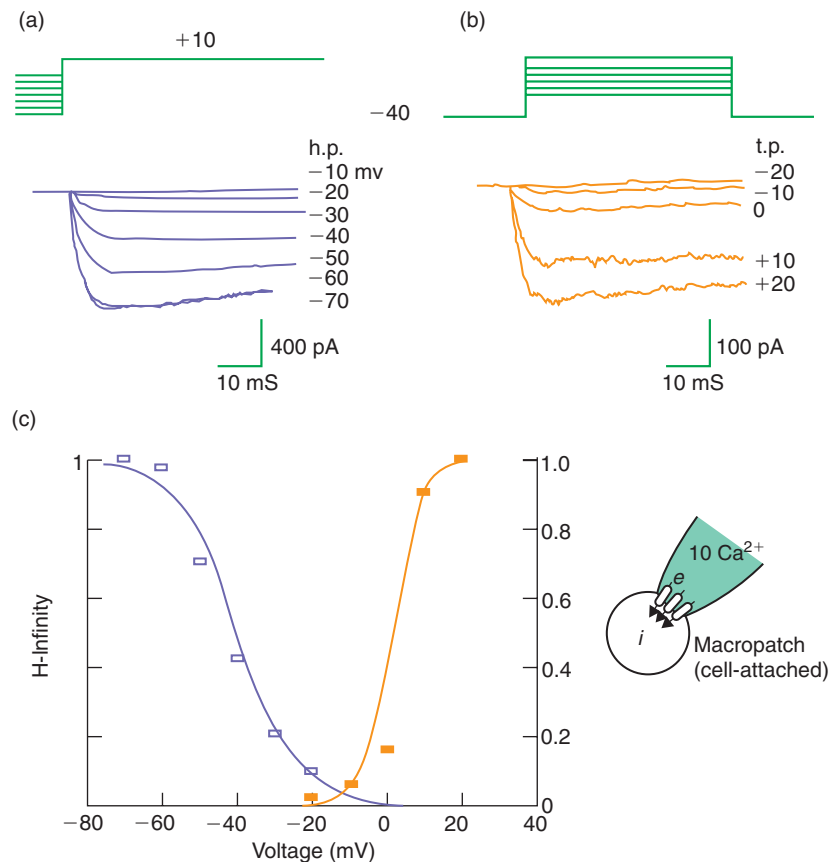


**FIGURE 5.13** Voltage dependence of activation and inactivation of the L-type  $\text{Ca}^{2+}$  current.

The macroscopic L current is recorded in a cell with very little T or N current. (a) Inactivation of the L current with holding potential: a test depolarization to +10 mV is applied from holding potentials (h.p.) varying from -70 to -10 mV. (b) Activation of the L current with depolarization: test depolarizations (t.p.) to -30, -20, -10, 0, +10 and +20 mV are applied from a holding potential of -40 mV. (c) Activation-inactivation curves obtained from the data in (b) and (a), respectively. The peak  $\text{Ca}^{2+}$  current amplitudes ( $I$ ) are normalized to the maximal current ( $I_{\text{max}} = 1$ ) obtained in each set of experiments and plotted against the holding (inactivation curve,  $\blacksquare$ ) or test potential (activation curve,  $\bullet$ ). For the activation curve, data are plotted as  $I = I_{\text{max}}\{1 + \exp [(V_{1/2} - V)/k]\}^{-1}$  and for the inactivation curve as  $I = I_{\text{max}}\{1 - \exp [(V - V_{1/2})/k]\}^{-1}$ .  $V_{1/2}$  is the voltage at which the current  $I$  is half-activated ( $I = I_{\text{max}}/2$  when  $V_{1/2} = 2$  mV) or half-inactivated ( $I = I_{\text{max}}/2$  when  $V_{1/2} = -40$  mV). All the recordings are performed in the presence of 10 mM  $\text{Ca}^{2+}$  in the recording pipette solution which bathes the extracellular side of the channels. Adapted from Fox AP, Nowycky M, Tsien RW (1987) Kinetic and pharmacological properties distinguishing three types of calcium currents in chick sensory neurones. *J. Physiol.* 394, 149–172, with permission.

In summary, L channels generate a large  $\text{Ca}^{2+}$  current that is activated by large depolarizations to 0/+10 mV and inactivates with a very slow time course during a step. N and P channels generate smaller  $\text{Ca}^{2+}$  currents that are activated with depolarization to -30/0 mV and inactivate or not during a depolarizing step.

The inactivation process of  $\text{Ca}^{2+}$  channels can be voltage-dependent, time-dependent and calcium-dependent. Voltage-dependent inactivation is observed by changing the holding potential (see **Figures 5.13a**, **5.14a** and **5.15a**). Time-dependent inactivation is observed during a long depolarizing step, in the presence of  $\text{Ba}^{2+}$  as the charge carrier (**Figure 5.16**).  $\text{Ca}^{2+}$ -dependent inactivation depends on the amount of  $\text{Ca}^{2+}$  influx through open  $\text{Ca}^{2+}$  channels. It can be considered as a negative feedback control of  $\text{Ca}^{2+}$  channels by  $\text{Ca}^{2+}$  channels.

### Calcium-dependent inactivation

Several lines of evidence point to the existence of a  $\text{Ca}^{2+}$ -induced inactivation of  $\text{Ca}^{2+}$  currents:

- The degree of inactivation is proportional to the amplitude and frequency of the  $\text{Ca}^{2+}$  current.
- Intracellular injection of  $\text{Ca}^{2+}$  ions into neurons produces inactivation.
- Intracellular injection of  $\text{Ca}^{2+}$  chelators such as EGTA or BAPTA reduces inactivation (**Figure 5.17**).
- Substitution of  $\text{Ca}^{2+}$  ions with  $\text{Sr}^{2+}$  or  $\text{Ba}^{2+}$  reduces inactivation.
- Very large depolarizations to near  $E_{\text{Ca}}$ , where the entry of  $\text{Ca}^{2+}$  ions is small, produce little inactivation.

Recordings of L and N channels in **Figures 5.13** and **5.14** were obtained with  $\text{Ca}^{2+}$  as the charge carrier and

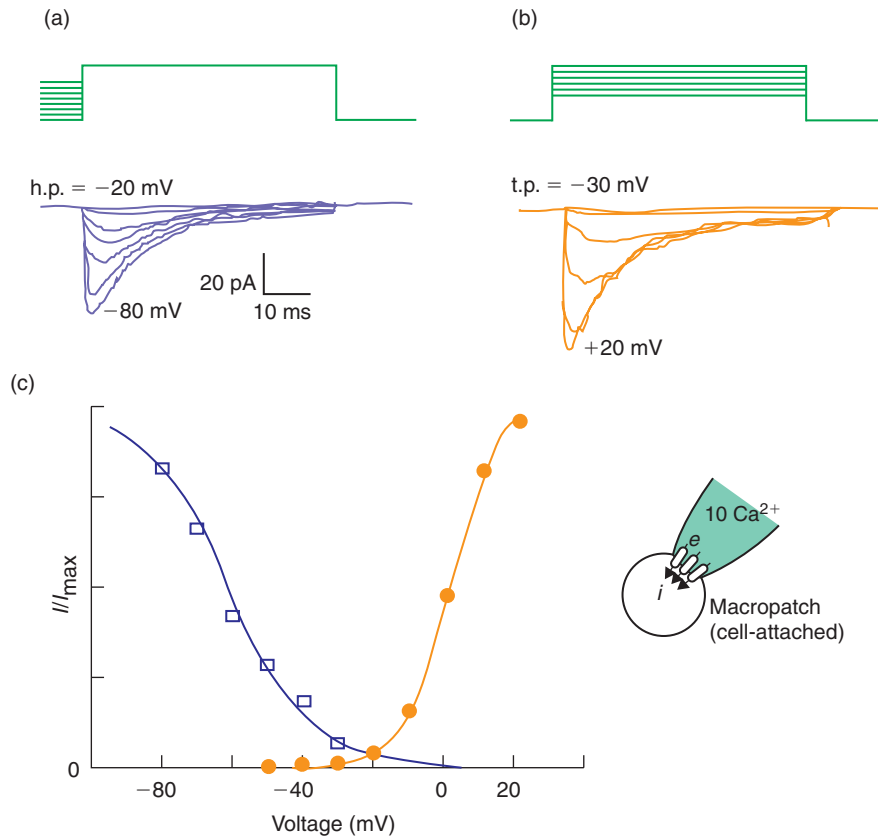


**FIGURE 5.14** Voltage dependence of activation and inactivation of the N-type  $\text{Ca}^{2+}$  current.

The macroscopic N current is recorded in cell-attached patches containing hundreds of channels (macropatch). (a) Inactivation of the N current with holding potential: test depolarization to +10 mV is applied from holding potentials (h.p.) varying from -70 to -10 mV. (b) Activation of the N current with depolarization: test depolarizations (t.p.) to -30, -20, -10, 0, +10 and +20 mV are applied from a holding potential of -80 mV. (c) Activation-inactivation curves obtained from the data in (b) and (a), respectively. The peak  $\text{Ca}^{2+}$  current amplitudes ( $I$ ) are normalized to the maximal current ( $I_{\max} = 1$ ) obtained in each set of experiments and plotted against the holding (inactivation curve,  $\blacksquare$ ) or test potential (activation curve,  $\bullet$ ). For the activation curve, data are plotted as  $I = I_{\max} \{1 + \exp [(V_{1/2} - V)/k]\}^{-1}$  and for the inactivation curve as  $I = I_{\max} \{1 + \exp [(V - V_{1/2})/k]\}^{-1}$ .  $V_{1/2}$  is the voltage at which the current  $I$  is half-activated ( $I = I_{\max} / 2$  when  $V_{1/2} = 1.5$  mV) or half-inactivated ( $I = I_{\max} / 2$  when  $V_{1/2} = -61.5$  mV). The number of channels is estimated as in Figure 5.12. Adapted from Fox AP, Nowycky MC, Tsien RW (1987) Single-channel recordings of three types of calcium channels in chick sensory neurones. *J. Physiol.* **394**, 173–200, with permission.

that of P channels in **Figure 5.15** with  $\text{Ba}^{2+}$  as the charge carrier. Therefore, the inactivation seen in **Figures 5.13** and **5.14**, results from three parameters: voltage, time and increase of intracellular  $\text{Ca}^{2+}$  concentration. In contrast, the inactivation of the P current observed in **Figure 5.15** is a voltage- and time-dependent process.

The macroscopic  $\text{Ca}^{2+}$  current of *Aplysia* neurons is recorded in voltage clamp. During depolarizing voltage steps, the  $\text{Ca}^{2+}$  current increases to a peak and then declines to a steady state  $\text{Ca}^{2+}$  current (a non-inactivating component of current). The buffering of cytoplasmic free  $\text{Ca}^{2+}$  ions with EGTA increases the amplitude of the peak current and that of the steady-state current (**Figure 5.17**). This shows that the increase of intracellular  $\text{Ca}^{2+}$  ions resulting from  $\text{Ca}^{2+}$  entry through  $\text{Ca}^{2+}$  channels causes  $\text{Ca}^{2+}$  current inactivation. It also shows that the

peak current is probably already decreased in amplitude owing to early development of inactivation.

### 5.3 THE REPOLARIZATION PHASE OF $\text{Ca}^{2+}$ -DEPENDENT ACTION POTENTIALS RESULTS FROM THE ACTIVATION OF $\text{K}^{+}$ CURRENTS $I_{\text{K}}$ AND $I_{\text{KCa}}$

The  $\text{K}^{+}$  currents involved in calcium spike repolarization are the delayed rectifier ( $I_{\text{K}}$ ) studied in Chapter 4 and the  $\text{Ca}^{2+}$ -activated  $\text{K}^{+}$  currents ( $I_{\text{KCa}}$ ). Meech and Strumwasser in 1970 were the first to describe that a microinjection of  $\text{Ca}^{2+}$  ions into *Aplysia* neurons activates a  $\text{K}^{+}$  conductance and hyperpolarizes the membrane.

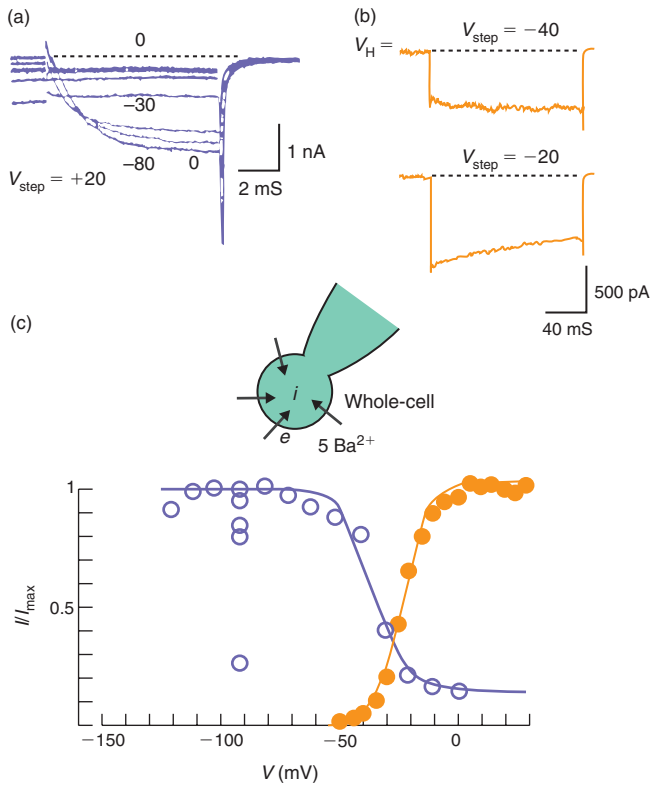


**FIGURE 5.15** Voltage dependence of activation and inactivation of the P-type  $\text{Ca}^{2+}$  current.

The macroscopic P current is recorded in Purkinje cells (whole-cell patch). The T-type  $\text{Ca}^{2+}$  current present in these cells is either absent or subtracted. (a) Inactivation of the P current with holding potential: a test depolarization to +20 mV is applied from holding potentials varying from -80 to 0 mV. (b) Activation of the P current with depolarization: test depolarizations ( $V_{\text{step}}$ ) to -40 and -20 mV are applied from a holding potential of -110 mV. (c) Activation-inactivation curves obtained from the data obtained in (b) and (a), respectively. The peak  $\text{Ca}^{2+}$  current amplitudes ( $I$ ) are normalized to the maximal current ( $I_{\text{max}} = 1$ ) obtained in each set of experiments and plotted against the holding (inactivation curve, ■) or test potential (activation curve, ●). For the activation curve, data are plotted as  $I = I_{\text{max}}[1 + \exp[(V_{1/2} - V)/k]]^{-1}$  and for the inactivation curve as  $I = I_{\text{max}}[1 + \exp[(V - V_{1/2})/k]]^{-1}$ .  $V_{1/2}$  is the voltage at which the current  $I$  is half-activated ( $I = I_{\text{max}}/2$  when  $V_{1/2} = -22$  mV) or half-inactivated ( $I = I_{\text{max}}/2$  when  $V_{1/2} = -34$  mV). In all recordings, the extracellular solution contains 5 mM  $\text{Ba}^{2+}$ . Adapted from Regan L (1991) Voltage-dependent calcium currents in Purkinje cells from rat cerebellar vermis. *J. Neurosci.* **11**, 2259–2269, with permission.

On the basis of these results, the authors postulated the existence of a  $\text{Ca}^{2+}$ -activated  $\text{K}^+$  conductance. The amount of participation of  $\text{Ca}^{2+}$ -activated  $\text{K}^+$  currents in spike repolarization depends on the cell type.

### 5.3.1 The $\text{Ca}^{2+}$ -activated $\text{K}^+$ currents are classified as big K (BK) channels and small K (SK) channels

Big K channels have a high conductance (100–250 pS depending on  $\text{K}^+$  concentrations) and are sensitive to

both voltage and  $\text{Ca}^{2+}$  ions so that their apparent sensitivity to  $\text{Ca}^{2+}$  ions is increased when the membrane is depolarized. Their activity is blocked by TEA and charybdotoxin, a toxin from scorpion venom. Small K channels have a smaller conductance (10–80 pS depending on  $\text{K}^+$  concentrations) and are insensitive to TEA and charybdotoxin but sensitive to apamin, a toxin from bee venom. It is a heterogeneous class containing both voltage-dependent and voltage-independent channels. Big K and small K channels are very selective for  $\text{K}^+$  ions over  $\text{Na}^+$  ions and are activated by increases in the concentration of cytoplasmic  $\text{Ca}^{2+}$  ions.

The channels originally termed ‘big’ potassium (BK) channels, are also called maxi-K channels or SLO family channels, a name derived from the conserved gene that encodes this channel, which was first cloned in *Drosophila melanogaster*. Voltage-clamp recordings of currents in the flight muscles of a *Drosophila* mutant with a severely lethargic phenotype, named *slowpoke*, revealed that the calcium-dependent component of the outward  $\text{K}^+$  current was absent, implicating the *slowpoke* (*slo*) gene as the structural locus encoding the channel protein. The mammalian *slo* orthologue *Slo1* was cloned by low-stringency DNA hybridization of a mammalian cDNA library using the *Drosophila slo* cDNA. The conserved protein domains of SLO1 seem to reflect separate mechanisms for voltage and  $\text{Ca}^{2+}$  sensing. The primary sequence consists of two distinct regions. The ‘core’ region (which includes hydrophobic segments S0–S6) resembles a canonical voltage-gated  $\text{K}^+$  channel except for the inclusion of the additional S0 segment (Figure 5.20a). The distal part of the carboxyl region (containing S9–S10), termed the tail, includes the region that is most highly conserved among SLO1 proteins from different species, the calcium bowl. The gating of SLO1 channels by both voltage and the binding of intracellular  $\text{Ca}^{2+}$  suggests that the two independent sensing mechanisms converge near the gates of the pore.

The genes that encode the SK channels belong to the KCNN gene family. SK channels have a similar topology to members of the voltage-gated (Kv)  $\text{K}^+$  channel superfamily. They consist of six transmembrane segments (S1–S6), with the pore located between S5 and S6. The S4 segment, which confers voltage sensitivity to the Kv channel, shows in SK channels a reduced number and a disrupted array of positively charged amino acids. The SK channels retain only two of the seven positively charged amino acids that are found in the S4 segment of Kv channels, and only one of these residues corresponds to the four arginine residues that carry the gating charges in Kv channels. These differences in the primary sequence could represent the molecular framework for the observed voltage independence of SK channels.

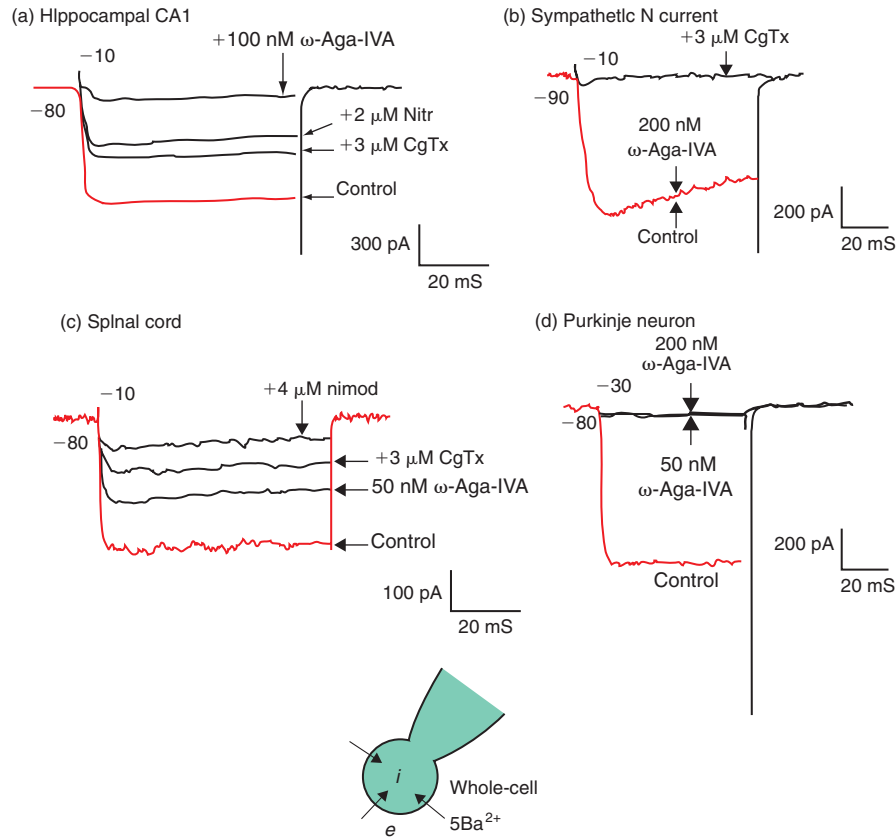


**FIGURE 5.16** Pharmacology of L-, N- and P-type  $\text{Ca}^{2+}$  channels.

The macroscopic mixed  $\text{Ca}^{2+}$  currents are recorded in different neurons with  $\text{Ba}^{2+}$  as the charge carrier (whole-cell patch). High-threshold  $\text{Ca}^{2+}$  currents are evoked by depolarizations to  $-30$  or  $-10$  mV from a holding potential of  $-90$  or  $-80$  mV. Various blockers or toxins are applied in order to block selectively one type of high-threshold  $\text{Ca}^{2+}$  current at a time:  $\omega$ -conotoxin (CgTx,  $3 \mu\text{M}$ ) selectively blocks N current, nitrendipine or nimodipine (nitr., nimod.,  $2\text{--}4 \mu\text{M}$ ) selectively blocks L current, and  $\omega$ -agatoxin ( $\omega$ -Aga-IVA,  $50\text{--}200$  nM) selectively blocks P current. In hippocampal cells of the CA1 region and in spinal cord interneurons, the high-threshold  $\text{Ca}^{2+}$  current is a mixed N, L and P current. In sympathetic neurons it is almost exclusively N and in Purkinje cells almost exclusively P. The intrapipette solution contains (in mM): 108 Cs methanesulphonate,  $4 \text{MgCl}_2$ , 9 EGTA, 9 HEPES, 4 MgATP, 14 creatine phosphate, 1 GTP; pH = 7.4. The extracellular solution contains (in mM):  $5 \text{BaCl}_2$ , 160 TEACL, 0.1 EGTA, 10 HEPES; pH = 7.4. Adapted from Mintz IM, Adams ME, Bean B (1992) P-type calcium channels in rat central and peripheral neurons. *Neuron* 9, 85–95, with permission.

### 5.3.2 $\text{Ca}^{2+}$ entering during the depolarization or the plateau phase of $\text{Ca}^{2+}$ -dependent action potentials activates $\text{K}_{\text{Ca}}$ channels

To study  $\text{Ca}^{2+}$ -activated  $\text{K}^+$  channels from rat brain neurons, plasma membrane vesicle preparation is incorporated into planar lipid bilayers. In such conditions, the activity of four distinct types of  $\text{Ca}^{2+}$ -activated  $\text{K}^+$  channels is recorded. We will look at one example of a big K and one example of a small K channel. This preparation allows the recording of single-channel activity (Figure 5.18).

The current–voltage relations obtained in the presence of two different extracellular  $\text{K}^+$  concentrations show that the current reverses at  $E_{\text{K}}$ , the theoretical reversal potential for  $\text{K}^+$  ions as expected for a purely  $\text{K}^+$ -selective channel. The  $\text{Ca}^{2+}$ -dependence is studied

by raising the intracellular  $\text{Ca}^{2+}$  concentration in the range of  $0.1\text{--}10 \mu\text{M}$ . Channels are activated by micromolar concentrations of  $\text{Ca}^{2+}$ . The open probabilities of the big K and small K channels are largely increased when the medium bathing the intracellular side of the membrane contains  $0.4 \mu\text{M}$   $\text{Ca}^{2+}$  instead of  $0.1 \mu\text{M}$  (Figures 5.19a, b). For comparison the  $\text{Ca}^{2+}$ -sensitivity of big K channels from cultured rat skeletal muscle is shown in Figure 5.19c. The rat brain big K channels are sensitive to nanomolar concentrations of charybdotoxin (CTX) and millimolar concentrations of extracellular TEA ions (Figure 5.20).

The macroscopic  $\text{Ca}^{2+}$ -activated  $\text{K}^+$  currents are recorded from a bullfrog sympathetic neuron in single-electrode voltage clamp mode ( $V_{\text{H}} = -28$  mV). The iontophoretic injection of  $\text{Ca}^{2+}$  ions via the recording

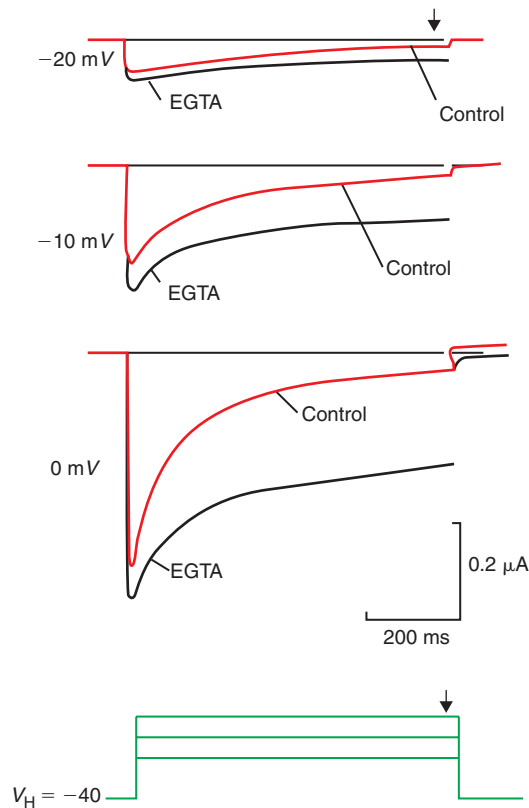


FIGURE 5.17 Intracellular EGTA slows  $\text{Ca}^{2+}$ -dependent inactivation of  $\text{Ca}^{2+}$  channels.

The macroscopic  $\text{Ca}^{2+}$  current is recorded in axotomized *Aplysia* neurons in double-electrode voltage clamp (axotomy is performed in order to improve space clamp). Control  $\text{Ca}^{2+}$  currents are recorded in response to step depolarizations to  $-20$ ,  $-10$  and  $0$  mV from a holding potential of  $-40$  mV (control traces). Iontophoretic ejection of EGTA ( $300$ – $500$  nA for  $4$ – $8$  min) increases the peak amplitude of the  $\text{Ca}^{2+}$  current and slows its inactivation at all potentials tested (EGTA traces). The amplitude of the non-inactivating component of the current is measured at the end of the steps (arrow). Adapted from Chad J, Eckert R, Ewald D (1984) Kinetics of calcium-dependent inactivation of calcium current in voltage-clamped neurons in *Aplysia californica*. *J. Physiol. (Lond.)* **347**, 279–300, with permission.

electrode triggers an outward current (Figure 5.21a). Its amplitude increases when the iontophoretic current is increased; i.e. when the amount of  $\text{Ca}^{2+}$  ions injected is increased. To study the voltage-dependence and the kinetics of activation of this  $\text{Ca}^{2+}$ -activated outward current, depolarizing steps from a holding potential of  $-50$  mV are applied in the presence of  $2$  mM of  $\text{Ca}^{2+}$  in the extracellular medium (Figure 5.21b, 2Ca). Suppression of  $\text{Ca}^{2+}$  entry by removal of  $\text{Ca}^{2+}$  ions from the extracellular medium ( $0\text{Ca}$ ) eliminates an early  $\text{Ca}^{2+}$ -activated outward current. In the  $\text{Ca}$ -free medium, only the sigmoidal delayed rectifier  $\text{K}^+$  current  $I_K$  is recorded. In the presence of external  $\text{Ca}^{2+}$

ions, both  $I_K$  and a  $I_{K(\text{Ca})}$  are recorded (Figure 5.21b, right). The recorded  $I_{K(\text{Ca})}$  corresponds to a big K current also called  $I_C$  in some preparations. It has activation kinetics sufficiently rapid to play a role in spike repolarization (Figure 5.22).

In nerve terminals at the motor end plate, big K channels are co-localized with voltage-dependent  $\text{Ca}^{2+}$  channels. They play an important role in repolarizing the plasma membrane following each action potential. This repolarization resulting from the increased activity of  $\text{Ca}^{2+}$ -activated  $\text{K}^+$  channels closes voltage-dependent  $\text{Ca}^{2+}$  channels and constitutes an important feedback mechanism for the regulation of voltage-dependent  $\text{Ca}^{2+}$  entry.  $I_{\text{Ca}}$  current thereby lowers intracellular  $\text{Ca}^{2+}$  concentration and dampens neurotransmitter secretion. Conversely when it is strongly reduced by TEA or apamin, transmitter release is increased.

## 5.4 CALCIUM-DEPENDENT ACTION POTENTIALS ARE INITIATED IN AXON TERMINALS AND IN DENDRITES

### 5.4.1 Depolarization of the membrane to the threshold for the activation of L-, N- and P-type $\text{Ca}^{2+}$ channels has two origins

L-, N- and P-type  $\text{Ca}^{2+}$  channels are high-threshold  $\text{Ca}^{2+}$  channels. This means that they are activated in response to a relatively large membrane depolarization. In cells (e.g. neurons, heart muscle cells) where the resting membrane potential is around  $-80$ /  $-60$  mV, a  $40$ – $60$  mV depolarization is therefore needed to activate the high-threshold  $\text{Ca}^{2+}$  channels. Such a membrane depolarization is too large to result directly from the summation of excitatory postsynaptic potentials (EPSPs). It usually results from a  $\text{Na}^+$  spike. In heart Purkinje cells,  $\text{Na}^+$  entry during the sudden depolarization phase of the action potential depolarizes the membrane to the threshold for L-type  $\text{Ca}^{2+}$  channel activation: the  $\text{Na}^+$ -dependent depolarization phase is immediately followed by a  $\text{Ca}^{2+}$ -dependent plateau (see Figure 4.2d). In axon terminals, the situation is similar: the  $\text{Na}^+$ -dependent action potential actively propagates to axon terminals where it depolarizes the membrane to the threshold potential for N- or P-type  $\text{Ca}^{2+}$  channel activation: a  $\text{Na}^+/\text{Ca}^{2+}$ -dependent action potential is initiated (see Figure 4.2c).

In cerebellar Purkinje neurons the situation is somehow different: dendritic P-type  $\text{Ca}^{2+}$  channels are opened by the large EPSP resulting from climbing fibre

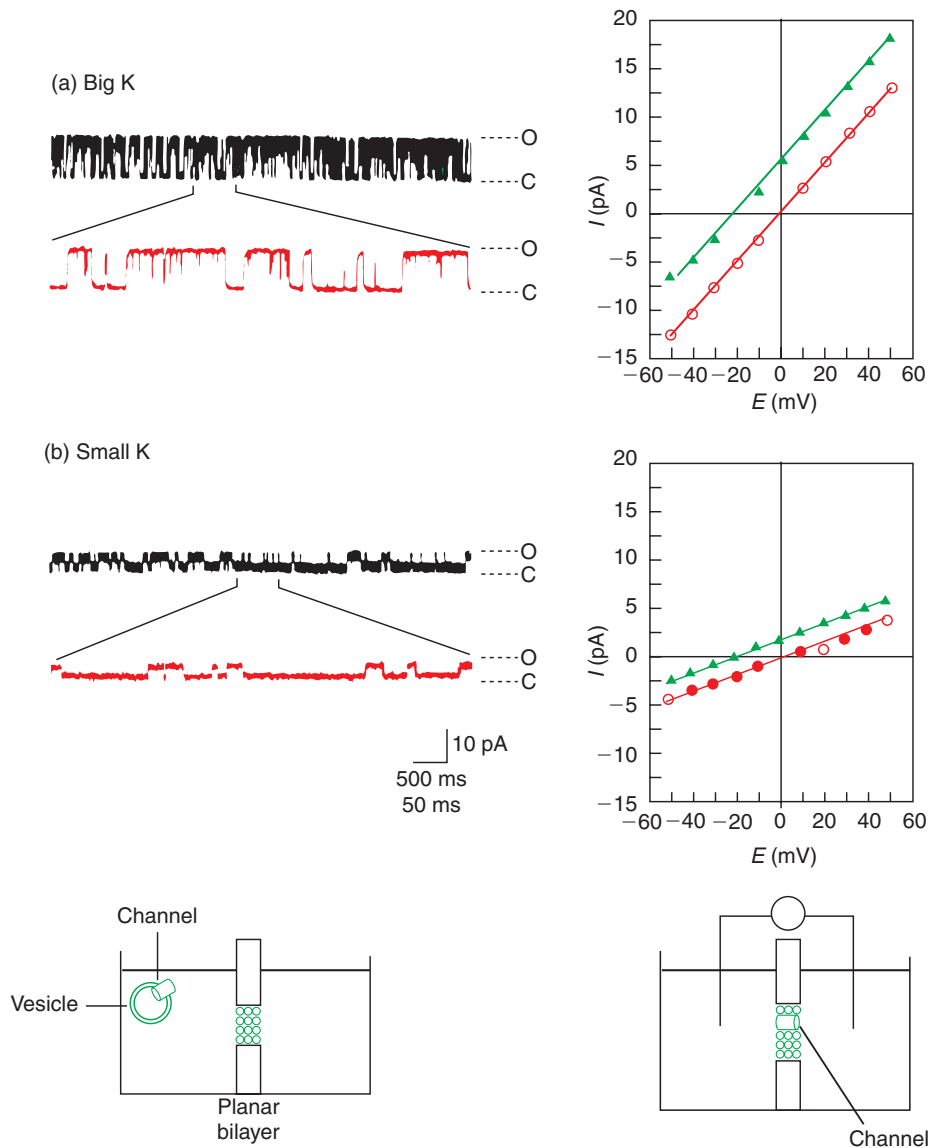


**FIGURE 5.18** Two types of rat brain  $\text{Ca}^{2+}$ -activated  $\text{K}^+$  channels incorporated into lipid bilayers. (a, b) Left: Single-channel recordings in symmetrical  $\text{K}^+$  (the extracellular and intracellular solutions contain 150 mM KCl) at  $V_H = 40$  mV. For all traces channel openings correspond to upward deflections. The recording length of upper traces is 6.4 s and each lower trace is expanded to show a 640 ms recording. Right:  $I/V$  relations for the big K channel and the small K channel in symmetrical  $\text{K}^+$  (150 mM, circles) and 150 mM KCl inside, 50 mM KCl outside (triangles). The slope conductance for each of these channels in symmetrical 150 mM KCl is 232 pS (big K channel) and 77 pS (small K channel). All the recordings are performed in the presence of 1.05 mM  $\text{CaCl}_2$  in the intracellular solution. Adapted from Reinhart PH, Chung S, Levitan IB (1989) A family of calcium-dependent potassium channels from rat brain. *Neuron* 2, 1031–1041, with permission. (a) Big K (rat brain neurons).

EPSP. As a result,  $\text{Ca}^{2+}$ -dependent action potentials are initiated and actively propagate in dendrites (see **Figure 4.2b**; also see Sections 16.2 and 17.3).

The cells that do not express voltage-gated  $\text{Na}^+$  channels and initiate  $\text{Ca}^{2+}$ -dependent action potentials (endocrine cells for example; see **Figure 5.1**) usually present a depolarized resting membrane potential

( $-50/-40$  mV) close to the threshold for L-type  $\text{Ca}^{2+}$  channel activation. In such cells, the activation of high-threshold  $\text{Ca}^{2+}$  channels results from a depolarizing current generated by receptor activation or from an intrinsic pacemaker current (for example, activation of the T-type  $\text{Ca}^{2+}$  current – see Section 14.2.2 – or the turning off of a leak  $\text{K}^+$  current).

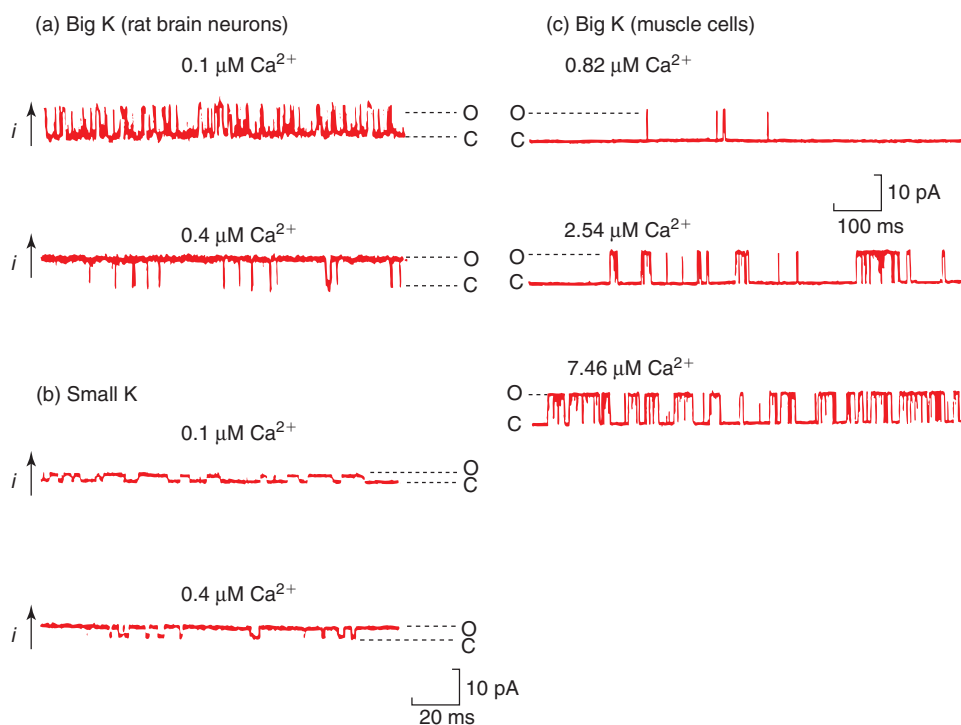


**FIGURE 5.19** Ca<sup>2+</sup>-dependence of Ca<sup>2+</sup>-activated K<sup>+</sup> channels.

(a, b) Single-channel activity of Ca<sup>2+</sup>-activated channels from the rat brain. The activity of the 232 pS big K channel and that of the 77 pS small K channel is recorded in the presence of 0.1 μM Ca<sup>2+</sup> (upper traces) and 0.4 μM Ca<sup>2+</sup> (lower traces) in symmetrical 150 mM KCl ( $V_H = +20$  mV). (c) Single-channel activity of a big K channel from rat skeletal muscle recorded at three different Ca<sup>2+</sup> concentrations in symmetrical 140 mM KCl ( $V_H = +30$  mV). O, open state; C, closed state. Part (a) from Chad J, Eckert R, Ewald D (1984) Kinetics of calcium-dependent inactivation of calcium current in voltage-clamped neurones in *Aplysia californica*. *J. Physiol. (Lond.)* **347**, 279–300, with permission. Part (b) adapted from McManus OB and Magleby KL (1991) Accounting for the calcium-dependent kinetics of single large-conductance Ca<sup>2+</sup>-activated K<sup>+</sup> channels in rat skeletal muscle. *J. Physiol.* **443**: 739–777, with permission.

#### 5.4.2 The role of the calcium-dependent action potentials is to provide a local and transient increase of $[Ca^{2+}]_i$ to trigger secretion, contraction and other Ca<sup>2+</sup>-gated processes

In some neurons, Ca<sup>2+</sup> entry through high-threshold Ca<sup>2+</sup> channels participates in the generation of various forms of electrical activity such as dendritic Ca<sup>2+</sup> spikes (Purkinje cell dendrites) and activation of Ca<sup>2+</sup>-sensitive channels such as Ca<sup>2+</sup>-activated K<sup>+</sup> or Cl<sup>-</sup> channels. However, the general role of Ca<sup>2+</sup>-dependent action potentials is to provide a local and transient increase of intracellular Ca<sup>2+</sup> concentration. Under normal conditions, the intracellular Ca<sup>2+</sup> concentration is very low, less than 10<sup>-7</sup> M. The entry of Ca<sup>2+</sup> ions through Ca<sup>2+</sup> channels locally and transiently increases the intracellular Ca<sup>2+</sup> concentration up to 10<sup>-4</sup> M. This local  $[Ca^{2+}]_i$  increase can trigger Ca<sup>2+</sup>-dependent intracellular events such as exocytosis of synaptic vesicles, granules or sliding of the myofilaments actin and myosin. It thus

couples action potentials (excitation) to secretion (neurons and other excitable secretory cells, see Chapter 7) or it couples action potentials to contraction (heart muscle cells). The influx of Ca<sup>2+</sup> also couples neuronal activity to metabolic processes and induces long-term changes in neuronal and synaptic activity. During development, Ca<sup>2+</sup> entry regulates outgrowth of axons and dendrites and the retraction of axonal branches during synapse elimination and neuronal cell death.

### 5.5 A NOTE ON VOLTAGE-GATED CHANNELS AND ACTION POTENTIALS

Voltage-gated Na<sup>+</sup>, K<sup>+</sup> and Ca<sup>2+</sup> channels of action potentials share a similar structure and are all activated by membrane depolarization. The Na<sup>+</sup>, Na<sup>+</sup>/Ca<sup>2+</sup> and Ca<sup>2+</sup> action potentials have a similar pattern: the depolarization phase results from the influx of cations, Na<sup>+</sup> and/or Ca<sup>2+</sup>, and the repolarization phase results from

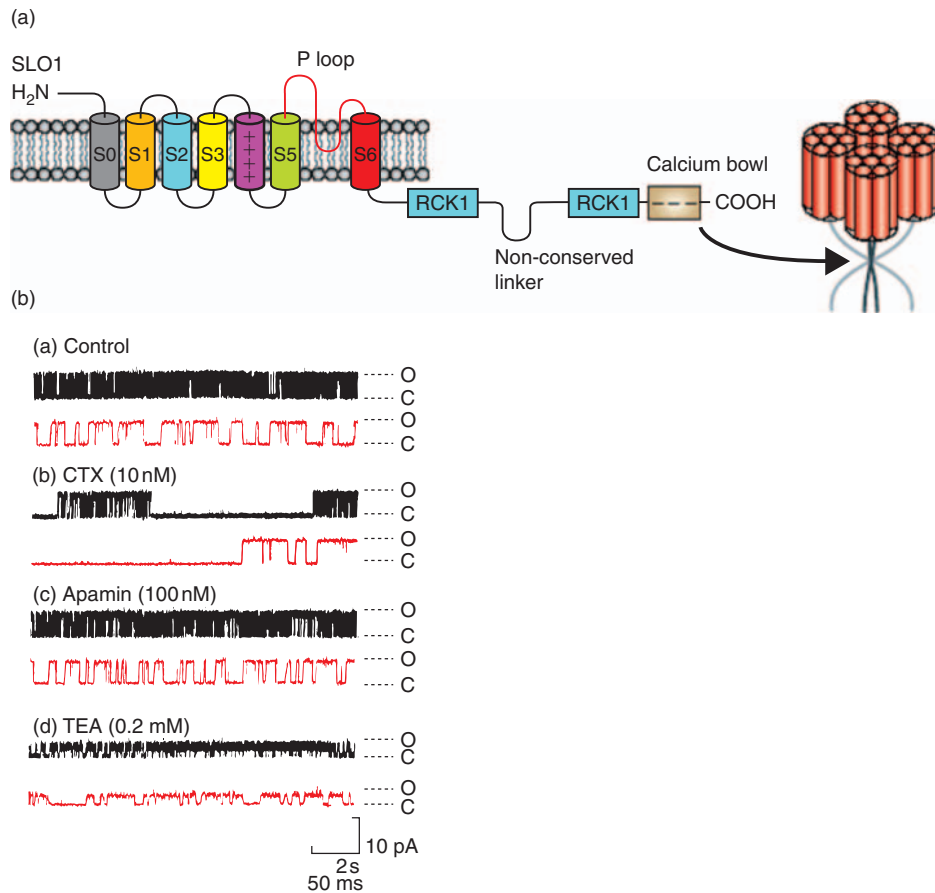


**FIGURE 5.20 The big K channel.**

(a) Schematic representation of SLO1  $\alpha$ -subunit. SLO1 subunit has an additional S0 membrane-spanning domain compared to delayed rectifier  $\text{K}^+$  channels and also includes an extensive cytosolic carboxy-terminal extension containing sites that sense cytosolic factors, such as the calcium bowl. RCK, regulators of conductance of  $\text{K}^+$  domain. (b) Single-channel activity of the big K channel (232 pS channel) in symmetrical 150 mM KCl at two different time bases ( $V_H = +40$  mV). From top to bottom: Control conditions. In the presence in the extracellular solution of, respectively, 10 nM charybdotoxin (CTX), 100 nM apamin, and 0.2 mM tetraethylammonium chloride (TEA). All the recordings are performed in the presence of 1.05 mM  $\text{Ca}^{2+}$  in the intracellular solution. Part (a) from Salkoff L, Ferreira G, Santi C, Wei A (2006) High-conductance potassium channels of the SLO family *Nature reviews. Neuroscience* 5, 921–931. Part (b) from Chad J, Eckert R, Ewald D (1984) Kinetics of calcium-dependent inactivation of calcium current in voltage-clamped neurones in *Aplysia californica*. *J. Physiol. (Lond.)* 347, 279–300, with permission.

the inactivation of  $\text{Na}^+$  or  $\text{Ca}^{2+}$  channels together with the efflux of  $\text{K}^+$  ions. However, these action potentials have at least one important difference. The  $\text{Na}^+$ -dependent action potential is all-or-none. In contrast the  $\text{Ca}^{2+}$ -dependent action potential is gradual. This reflects different functions. The  $\text{Na}^+$ -dependent action potential propagates over long distances *without attenuation* in order to transmit information from soma-initial segment to axon terminals where they trigger  $\text{Ca}^{2+}$ -dependent action potentials.  $\text{Ca}^{2+}$ -dependent action potentials have

the general role of providing a local, *gradual* and transient  $\text{Ca}^{2+}$  entry.

## FURTHER READING

- Catterall WA (2000). Structure and regulation of voltage-gated  $\text{Ca}^{2+}$  channels. *Annu. Rev. Cell Dev. Biol.* 16, 521–555.  
 Coetzee WA, Amarillo Y, Chiu J *et al.* (1999) Molecular diversity of  $\text{K}^+$  channels. *Ann. NY Acad. Sci.* 868, 233–285.

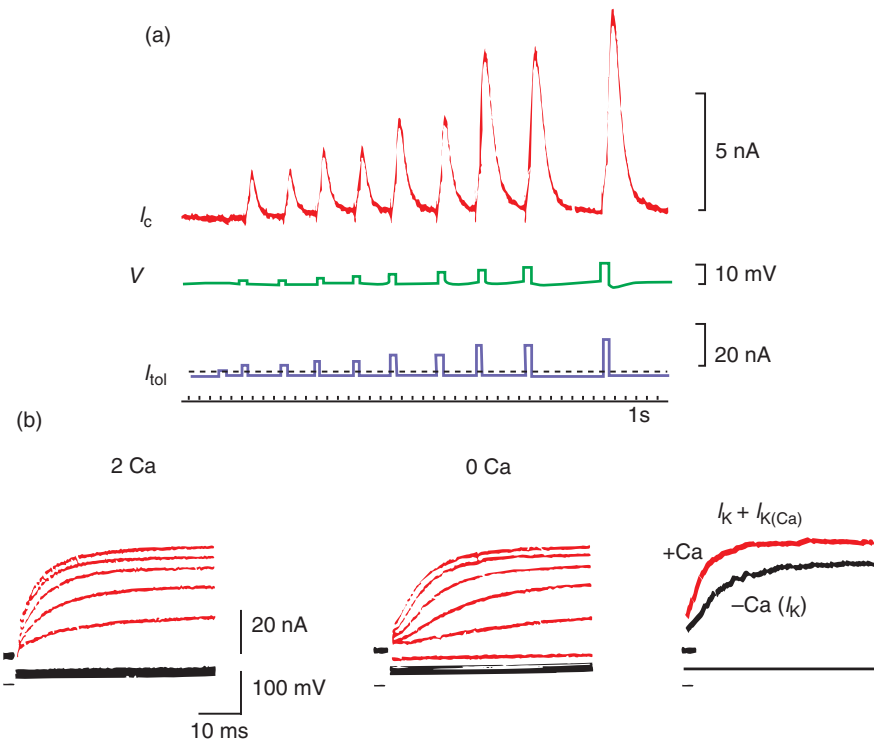


**FIGURE 5.21** The macroscopic  $\text{Ca}^{2+}$ -activated  $\text{K}^+$  current of bullfrog sympathetic neurons. (a) Outward currents recorded in single-electrode voltage clamp at a holding potential of  $-28$  mV. In response to increasing  $0.4$  s intracellular iontophoretic injections of  $\text{Ca}^{2+}$  from a microelectrode containing  $200$  mM  $\text{CaCl}_2$ , increasing outward currents are recorded. (b) Outward currents recorded during voltage steps to  $-20$ ,  $-10$ ,  $0$  and  $+20$  mV from a holding potential of  $-50$  mV in the presence of  $2$  mM external  $\text{Ca}^{2+}$  ( $2$  Ca) and a  $\text{Ca}$ -free external medium ( $0$  Ca). The leak current is subtracted. The two superimposed current traces recorded at the same potential in the presence ( $+ \text{Ca}$ ) or absence ( $- \text{Ca}$ ) of external  $\text{Ca}^{2+}$  ions show that an early component of the outward current is present ( $I_{\text{K}(\text{Ca})}$ ) in the presence of  $\text{Ca}^{2+}$  ions. Adapted from Brown DA, Constanti A, Adams PR (1983)  $\text{Ca}^{2+}$ -activated potassium current in vertebrate sympathetic neurons. *Cell Calcium* 4, 407–420, with permission.

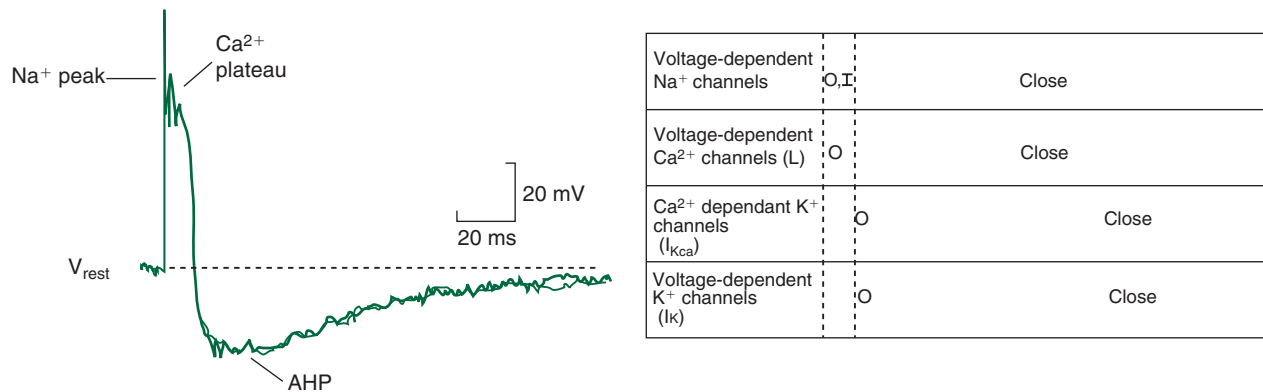


**FIGURE 5.22** States of voltage-gates  $\text{Na}^+$ ,  $\text{Ca}^{2+}$  and  $\text{K}^+$  channels. Different states in relation to the various phases of the  $\text{Na}^+/\text{Ca}^{2+}$ -dependent action potential. Example of the action potential recorded in olivary neurons of the cerebellum.

- De Leon M, Wang Y, Jones J *et al.* (1995) Essential  $\text{Ca}^{2+}$ -binding motif for  $\text{Ca}^{2+}$ -sensitive inactivation of L-type  $\text{Ca}^{2+}$  channels. *Science* **270**, 1502–1506.
- Denk W, Piston DW, Webb WW (1995) Two-photon molecular excitation in laser-scanning microscopy. In Pawley JB (ed.) *Handbook of Biological Microscopy*. New York: Plenum Press.
- Elkins T, Ganetzky B, Wu CF (1986) A *Drosophila* mutation that eliminates a calcium-dependent potassium current. *Proc. Natl Acad. Sci. USA* **83**, 8415–8419.
- Ertel EA, Campbell KP, Harpold MM *et al* (2000) Nomenclature of voltage-gated calcium channels. *Neuron* **25**, 533–535.
- Grynkiewicz G, Poenie M, Tsien RY (1985) A new generation of calcium indicators with greatly improved fluorescence properties. *J. Biol. Chem.* **260**, 3440–3448.
- Hodgkin AL and Huxley AF (1952) A quantitative description of membrane current and its application to conduction and excitation in nerve. *J. Physiol. (Lond.)* **117**, 500–544.
- Miller C (1995) The charybdotoxin family of  $\text{K}^+$  channel-blocking peptides. *Neuron* **15**, 5–10.
- Neher E and Augustine GJ (1992) Calcium gradients and buffers in bovine chromaffin cells. *J. Physiol. (Lond.)* **450**, 273–301.
- Schreiber M, Yuan A, Salkoff L (1999) Transplantable sites confer calcium sensitivity to BK channels. *Nature Neurosci.* **2**, 416–421.
- Stocker M (2004)  $\text{Ca}^{2+}$ -activated  $\text{K}^+$  channels: molecular determinants and function of the SK family. *Nature Reviews Neuroscience* **5**, 758–770.
- Stotz SC and Zamponi GW (2001) Structural determinants of fast inactivation of high voltage-activated  $\text{Ca}^{2+}$  channels. *Trends in Neurosciences* **24**, 176–181.
- Tan YP, Llano I, Hopt A, Wuerrlihausen F, Neher E (1999) Fast scanning and efficient photodetection in a simple two-photon microscope. *J. Neurosci. Meth.* **92**, 123–135.
- Tsien RY (1989) Fluorescent probes of cell signalling. *Ann. Rev. Neurobiol.* **12**, 221–253.
- Zamponi GW, Bourinet E, Nelson D, Nargeot J, Snutch TP (1997) Crosstalk between G proteins and protein kinase C mediated by the calcium channel  $\alpha_1$  subunit. *Nature* **385**, 442–446.
- Zhong H, Li B, Scheuer T, Catterall WA (2001) Control of gating mode by a single amino acid residue in transmembrane segment IS3 of the N-type  $\text{Ca}^{2+}$  channel. *PNAS* **98**, 4705–4709.

## APPENDIX 5.1 FLUORESCENCE MEASUREMENTS OF INTRACELLULAR $\text{Ca}^{2+}$ CONCENTRATION

### A5.1.1 The physical basis of fluorescence

#### *The interaction of light with matter*

Light is electromagnetic radiation that oscillates both in space and time, and has electric and magnetic field components that are perpendicular to each other. If for the sake of simplicity one focuses only on the electromagnetic component, it can be seen that the molecule, which is much smaller than the wavelength of light, will be perturbed by light because its electronic charge distribution will be altered by the oscillating electric field component of the light. Without resorting to complicated quantum mechanical calculations we can say that light will interact with matter via a resonance

phenomenon; i.e. the matter will absorb light only if the energy of the incoming photon is exactly equal to the difference between the potential energy of the lowest vibrational level of the ground state and that of one of the vibrational levels of the first excited state (**Figure A5.1**). The absorption of light therefore occurs in discrete amounts termed quanta. The energy  $E$  in a quantum of light (a photon) is given by:

$$E = h\nu = hc/\lambda,$$

where  $h$  is Planck's constant,  $\nu$  and  $\lambda$  are the frequency and wavelength of the incoming light, and  $c$  is the speed of light in a vacuum. When a quantum of light is absorbed by a molecule, a valence electron will be boosted into a higher energy orbit, called *the excited state*. This phenomenon will take place in  $10^{-15}$  s, resulting in conservation of the molecular coordinates. For the sake of simplicity the rotational energy levels are not taken into account and it is assumed that at room temperature the electrons will be at their lowest vibrational energy level.

The difference of energy between the vibrational levels being typically in the order of  $10 \text{ kcal mol}^{-1}$ , there is not enough thermal energy to excite a transition to higher vibrational levels at room temperature. One might thus assume that most of the electrons will lie at the lowest vibrational level of the ground state  $S_0 = 0$  (S for singlet, as the electrons spins are antiparallel). Because absorptive transitions occur to one of the vibrational levels of the excited state, had there been no interaction with the solvent molecules one could have measured the energy difference between the ground state and each of the vibrational levels of the excited

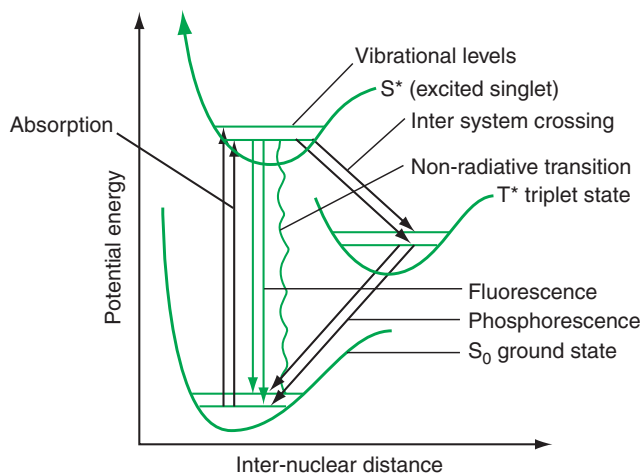


**FIGURE A5.1** Pathways to excitation and de-excitation of an electron.

The rotational levels between the vibrational levels and higher excited states are not shown for the sake of simplicity.

state. This type of spectra can only be obtained for chemical compounds in the gaseous state. The absorption spectra under those circumstances would resemble narrowly separated bands; however, the interaction of the orbital electrons with solvent molecules will broaden those peaks, producing the absorption spectra of the more familiar form.

### The return from the excited state

The electrons that have been promoted to one of the vibrational levels of the excited state will lose their vibrational energy through interaction with solvent molecules by a process known as *vibrational relaxation*. This process has a timescale much shorter than the lifetime of the electrons in the excited state ( $10^{-9}$  to  $10^{-7}$  s for aromatic molecules). The electrons that have been promoted to the excited state will return to the ground state from the lowest-lying excited vibrational state, by one of the following ways.

### Fluorescence emission

Some of the electrons in the excited state will return to one of the vibrational levels of the ground state by a radiative transition, whose frequency will be a function of the energy difference separating these levels. If one simply assumes that the energy spacing the vibrational levels of the excited and ground states are similar, one expects the fluorescence emission spectrum to be a mirror image of the absorption spectrum (**Figure A5.2**).

A further expectation will be that the  $S_{v=0}$  to  $S_{v=0}^*$  absorption will be at the same frequency as the  $S_{v=0}^*$  to  $S_{v=0}$  emission; however, this is rarely the case, as the absorption process takes place in about  $10^{-15}$  s. The orientation of the solvent molecules with respect to the electronic states will be conserved as well as the quantum coordinates of the molecule; however, as the

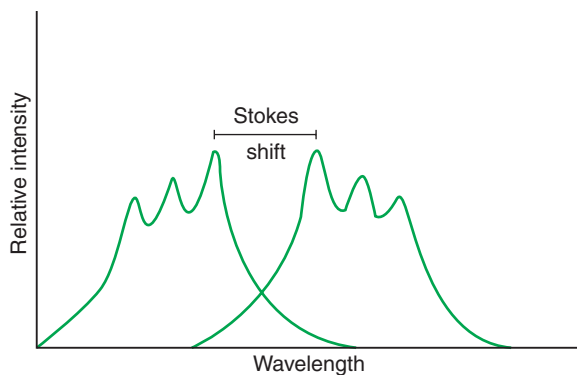


**FIGURE A5.2** Excitation (left) and emission (right) spectra of a hypothetical molecule.

The excitation spectrum has the same peaks as the absorption spectrum; the separation between the individual peaks reflects the potential energy differences between the vibrational levels.

excited level lifetimes are rather long, the solvent molecules will reorient favourably about the electronic levels, resulting in a difference in the zero-zero frequencies. This difference between  $S_{v=0}$  to  $S_{v=0}^*$  absorption and  $S_{v=0}^*$  to  $S_{v=0}$  emission is termed the *Stoke's shift*.

### Non-radiative transition

In this process the excitation energy will be lost mainly by interactions with solvent molecules, resulting in some of the electrons of the excited state returning to the ground state with a non-radiative transition. This process is favoured by an increase in temperature, and can explain why increasing the temperature causes a decrease in fluorescence intensities.

### Quenching of the excited state

The excitation energy might be lost through interactions, in the form of collisions of quenchers with the electrons in the excited orbital. Typical quenchers such as  $\text{O}_2$ ,  $\text{I}^-$  and  $\text{Mn}^{2+}$  ions will quench every time they collide with an excited singlet.

### Intersystem crossing

Intersystem crossing is a mechanically forbidden quantum process that occurs by a spin exchange of the electron of the excited singlet state, resulting in an excited triplet state  $\text{T}^*$  (**Figure A5.1**). As this process involves a forbidden transition its probability of occurrence will be extremely low; nevertheless it will occur because the potential energy of the excited triplet is usually lower than that of the excited singlet state. The electron in the excited triplet state can then become de-excited by a non-radiative transition, quenching, or by a radiative transition called *phosphorescence* (the light emitted will be of longer wavelength than fluorescence because of the lower potential energy of the excited triplet). One should note that the return to the ground state necessitates a novel forbidden transition  $\text{T}^*_{v=0}$  to  $S_{v=x}$  ( $x$  for any vibrational level of the ground state). The probability of this transition will be extremely low, for the same reasons given above, resulting in a long lifetime of the excited triplet state (seconds to days). This long-lived triplet state will result in a very weak intensity of radiation, will be prone to quenching by collisions with quenchers, and the non-radiative processes will compete well with the phosphorescence. Phosphorescence in solution will rarely be observed. In order to observe phosphorescence at all, one must rigorously remove oxygen from the medium, and should use rigid glasses at very low temperatures, in order to minimize the competing non-radiative processes.

Some of the electrons that have undergone intersystem crossing, and therefore are in the  $\text{T}^*_{v=0}$  state, may

undergo a novel intersystem crossing to the  $S^*$  level by the thermal energy provided by the solution, provided the energy difference between the  $T^*$  and  $S^*$  states is small; the return from the  $S^*_{v=0}$  to  $S^*_{v=x}$  level by fluorescence emission is called *delayed fluorescence* and has the effect of lengthening the fluorescence lifetime of the molecule beyond what is expected in normal fluorescence emissions.

### Photolysis: bleaching and toxicity

The molecules in the excited state undergo certain chemical reactions resulting in the loss of fluorescence; this is called *photobleaching*. It is estimated that a good organic fluorophore can be excited about  $10^4$  to  $10^5$  times before it bleaches. Some of the reaction products might be damaging for the cell, resulting in phototoxicity. One of the important ingredients in bleaching is the interaction between the triplet state of the fluorophore (**Figure A5.1**) and molecular oxygen ( $\text{O}_2$ ). The triplet state can transfer its energy to oxygen and bring it to its singlet excited state. Singlet oxygen is a reactive molecule that participates in many kinds of chemical reactions with organic molecules. As a result, the fluorophore loses its ability to fluoresce (it bleaches). In addition, the singlet oxygen can interact with other organic molecules causing phototoxicity for living cells. The minimal intensity of excitation and the minimal exposure time must be used in order to keep photobleaching and phototoxicity to a minimum.

### A5.1.2 Fluorescence measurements: general points

#### *Advantages*

In the absence of fluorophore, provided there is no background fluorescence, the level of the signal is zero, so that even a very small change of fluorescence of the fluorophore is detected. This might need a large amplification, itself limited by the noise level of the amplifier chain.

#### *Observation of fluorescence emission*

The best fluorimeter should maximize collection of the fluorescence emission and minimize collection of excitation light. This is usually achieved by selecting a band of excitation wavelengths located outside the emission spectrum using filters (interference or combination filters), or monochromator on the excitation side and highpass or bandpass filters on the emission side. The emission-side filters pass wavelengths longer than the excitation wavelengths (remember the Stoke's shift).

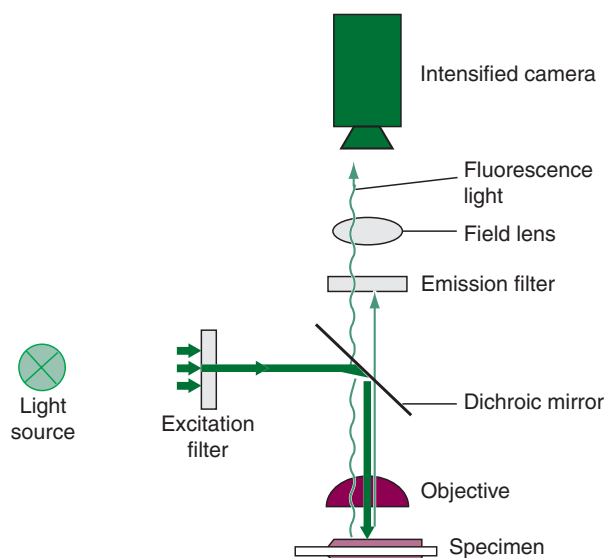


FIGURE A5.3 Epi-illumination microscopy.

For the measurement of fluorescence from individual cells, epi-illuminated fluorescence microscopes are used. The epiluminescence technique means that both the excitation and emission light have a common optical path through the objective. The key element of epi-illumination is the dichroic mirror; an interference mirror formed by successive depositions of dielectric layers on a transparent substrate. The dichroic mirror reflects the wavelengths below its cutoff frequency and transmits those that are above the cutoff. This cutoff frequency is chosen so that it reflects all of the excitation wavelengths, and transmits most of the emission wavelengths. The Stoke's shift is an aid in this respect. It is also possible to find polychroic mirrors that allow the simultaneous detection of many chromophores (**Figure A5.3**).

#### *Confocal and multiphoton microscopy*

The principle of confocal imaging was developed by Marvin Minsky in the mid-1950s. In a conventional (i.e., wide-field) fluorescence microscope, the entire specimen is flooded in light from a light source. All parts of the specimen throughout the optical path are excited and the fluorescence detected by a photodetector or a camera. The confocal microscope uses a laser to provide the excitation light (in order to get very high intensity of excitation and high resolution). The laser beam reflected from the dichroic beam splitter hits two mirrors which are mounted on motors and scan the sample. Dye in the sample fluoresces and the emitted light captured by the objective lens (epi-fluorescence) gets de-scanned by the same moving mirrors. The

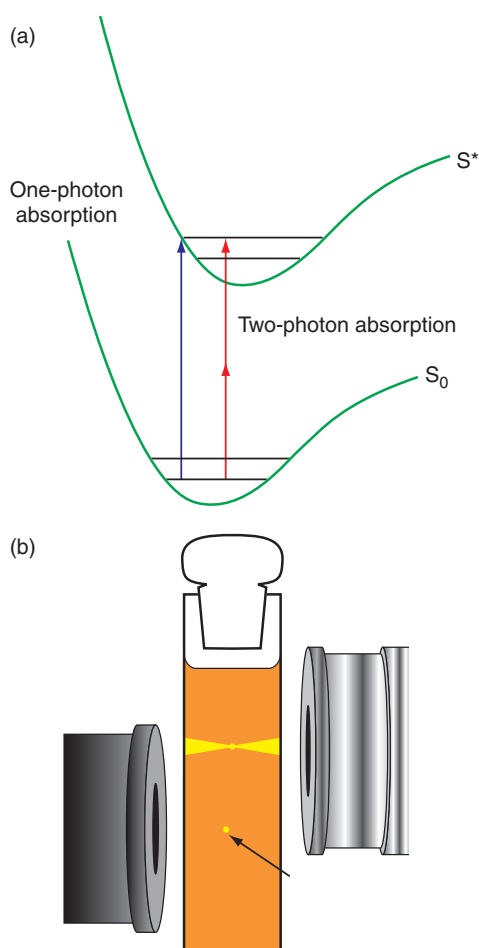


FIGURE A5.4 Comparison of one-photon and two-photon absorption.

(a) Two photons in the red (right) combine their energies to get absorbed as a one blue photon (left). The energies of the photons can be thought as equal to the amplitude of the vectors. The two photons that get absorbed need not have equal energies. (b) Fluorescence emission profile produced by one-photon absorption occurs throughout the laser beam focused in a fluorescent solution by the objective on the right. With the two-photon scheme, excitation is limited to the focal point of the objective on the left (shown by the arrow) providing inherent 3-dimensional resolution.

fluorescence passes through the dichroic and is focused onto the pinhole in an optically conjugate plane. The pinhole in front of the detector eliminates out-of-focus light. Only the fluorescence within the focal plane is detected by the detector, i.e. a photomultiplier tube. In fact, there is not a complete image of the sample at any given instant; only one point of the sample is observed (laser scanning confocal microscopy: LSCM). The detector is connected to a computer which builds up the image, one pixel at a time. In practice, this can be done around twice per second for a  $512 \times 512$  pixel image. The time limitation is due to the scanning mirrors. Several new features have been

recently developed to improve speed performance (spinning nipkow disc, multibeam excitation, lined 'pinhole' etc).

The resolution improvement due to confocal microscopy, either in  $xy$  or in  $z$  dimension, and the general use of laser as light source, represent a real revolution in imaging biological material. Despite these benefits, the confocal approach presents some limitations for specific applications such as deep imaging or long duration experiments in living tissue. Indeed, biological tissues strongly scatter visible light and prevent more than  $100\ \mu\text{m}$  depth images by defect of excitation light. On the other hand, increasing the laser power is not the solution because thermal and photolysis effects will definitively affect the sample. Despite the fact that laser beam excites only the fluorophores in its path, scanning the sample induces a large photobleaching effect in the entire light cone (Figure A5.4b). One has to deal with the laser power for the preservation of the sample.

In order to alleviate some of these limitations Denk *et al.* in 1990 took advantage of an old physical theoretic prediction and of new powerful pulsed lasers to develop multiphoton microscopy. In 1931, Maria Goeppert-Mayer predicted the possibility of simultaneous absorption by a molecule of two photons of long wavelength, combining their energies to cause the transition of the molecule to the excited state (remember that the energy of a photon is inversely proportional to its wavelength  $\lambda$ :  $E = hc/\lambda$ ). This can be viewed as two IR (near infrared) photons being absorbed simultaneously by a molecule normally excited by UV (Figure A5.4a). This technique, however, did not find practical use until the advent of very short pulse-width lasers for the following reasons.

The probability of two-photon absorption is  $\sim 10^{31}$  times lower than the probability of one-photon absorption, and therefore does not occur under normal illumination conditions. Typical cross-sections for one-photon absorption are of the order of  $10^{-16}\ \text{cm}^2$ ; for the two-photon case they are  $10^{-48}\ \text{cm}^4\ \text{s}^{-1}$ . The two-photon cross-sections are cited in GM (Goeppert-Mayer) units, with 1 GM being  $10^{-50}\ \text{cm}^4\ \text{s}^{-1}$ . In order for this absorption to occur, very high density photon fluxes confined to a small volume are needed. This was made possible by the advent of pulsed lasers, which typically generate pulses of 70 to 100 femtoseconds ( $1\ \text{fs} = 10^{-15}\ \text{s}$ ) width, each at power levels of 500 kW (1–3 W in average) and repetition rates of 80 MHz. For fluorescence measurements of biological samples, 10 mW laser intensity on the specimen plane are typically used. Under these conditions the excitation is confined to the focal volume only, as the necessary photon flux can only be reached at this plane. This has two very important implications: (i) as the excitation is limited to the focal plane, the

emission is also limited to this plane (**Figure A5.4b**), resulting in an intrinsic 'confocal' image. At this time, image reconstruction does not need any pinhole and allows the use of 'non-descanned' detectors placed just after the condenser or the objective (transmission or epifluorescence). This short-length optical tract is several times more efficient than the confocal one to collect emitted fluorescence and greatly improves recorded signals; (ii) other chromophores in the light cone are not excited, so photodamage and phototoxicity resulting from photolysis of the chromophore are greatly reduced. Light at long wavelengths is less prone to scattering and better penetrates biological tissue, enabling researchers to measure  $\text{Ca}^{2+}$  dynamics in a non-invasive way and from deeper locations. It is possible to measure  $\text{Ca}^{2+}$  signals from rat brain at a depth of  $800\ \mu\text{m}$  from the surface. Absorption is not limited to two photons only. Triple-photon absorption by UV dyes (DAPI...) or by nucleic acids with cross-sections as large as  $10^{-75}\ \text{cm}^6\ \text{s}^{-2}$  has been reported. This technique currently has the drawback of requiring rather expensive lasers, but one can expect prices to come down in the future, allowing their routine use.

### A5.1.3 Measurement of ion concentration by fluorescence techniques

The main requirement for an indicator to report the concentration of an ion is a change in its optical properties, and at the same time it must be highly specific for the ion in question, at physiological pH values. Furthermore, its binding and release from the ion must be faster than the kinetics of the intracellular ionic changes. Its affinity to that ion should be compatible with physiological conditions and prevent buffering effect. One can therefore envisage the production of probes that will change their absorption, bioluminescence (such as aequorin) or fluorescence properties as a function of ion concentration. Fluorescence is the technique of choice because of its higher sensitivity. In fluorescence measurements, the change in optical property sought to report an ionic concentration might be a change in quantum yield, excitation spectra or emission spectra.

#### Indicators for $\text{Ca}^{2+}$

Richard Tsien and colleagues have developed many probes sensitive to the free  $\text{Ca}^{2+}$  ions concentration. The common property of these probes is that they are all fluorescent derivatives of the calcium chelator BAPTA, which in turn is an aromatic analogue of the commonly used calcium chelator (EGTA, ethyleneglycol bis (13-aminoether) -N,N,N',N' tetra-acetic acid) (**Figure A5.5**). The probes form an octahedral complex,

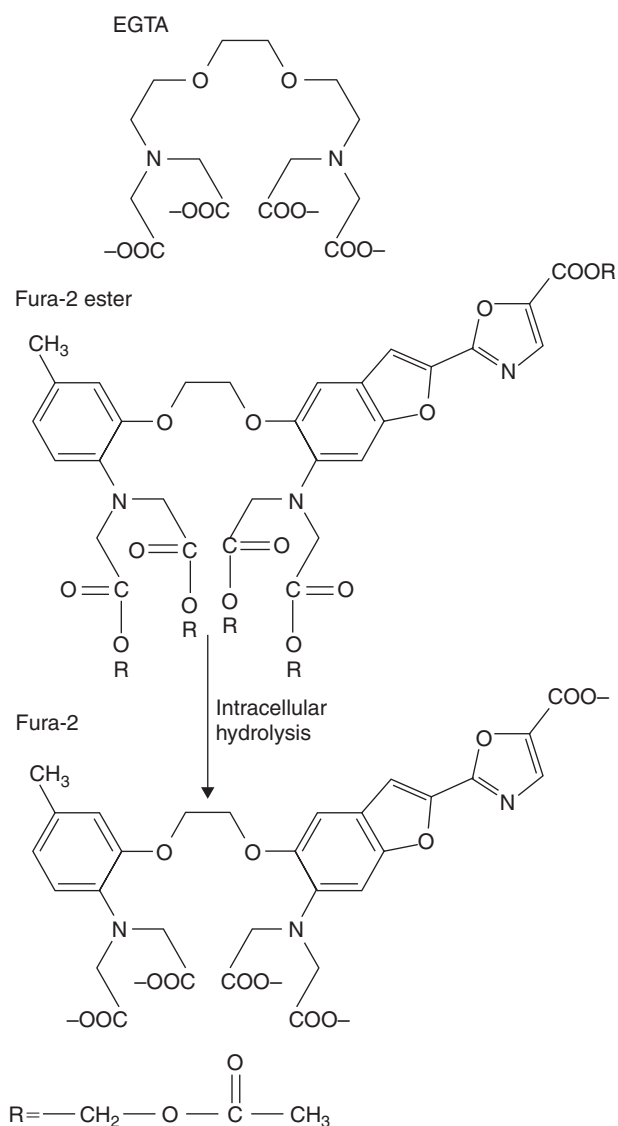


**FIGURE A5.5** Chemical structure of Fura-2.

Note the similarities between Fura-2 and the acetoxymylester variety Fura-2AM and EGTA. The AM variety is membrane permeant, and is de-esterified by intracellular esterases, liberating Fura-2, formaldehyde and acetate ions.

with the calcium ion at the centre of the plane formed by the  $\text{COO}^-$  groups of the carboxylic acid. The binding and unbinding of the ion induces a strain or relaxation on the electron cloud of the aromatic groups, which in turn results in changes of the spectral properties of the reporter chromophore.

Once these probes synthesized, several strategies were developed to make them penetrate in the cell, including direct injection of the chromophore salt through the patch clamp pipette allowing  $\text{Ca}^{2+}$  measurement combined with electrophysiological monitoring from a single neuron. Another way is to neutralize

carboxylic groups with ester residues to form acetoxy-methylester variety (AM). This neutral molecule diffuses through the plasma membrane and is de-esterified enzymatically to produce functional chromophore (**Figure A5.5**), this is convenient to load a population of cell either *in vivo* or *in vitro*.

Three such reporter chromophores have found much use in the measurement of intracellular free  $\text{Ca}^{2+}$  concentrations, namely INDO, Fura-2, and FLUO-3. Each of these probes has a certain number of advantages over the others, depending on the measurement technique sought. INDO and Fura-2 are ratiometric probes; i.e. the change in spectral properties occur at two different wavelengths, and by measuring the fluorescence intensities at these two wavelengths and taking their ratio; one can calculate the absolute value of the free  $\text{Ca}^{2+}$  ion concentration within the cytosol, given by the following formula (see Grynkiewicz *et al.*, 1985):

$$[\text{Ca}^{2+}] = K_i \{ (R - R_{\min}) / (R_{\max} - R) \},$$

where  $R_{\min}$  is the ratio at two wavelengths at zero ion concentration,  $R_{\max}$  is the ratio at 'infinite' ion concentration,  $R$  is the ratio of the measurements, and  $K_i$  is constant unifying instrumental parameters together with the  $K_D$  of the chromophore for calcium. The major advantage of ratiometric probes is the fact that they are insensitive to the intensity of the emitted light, which changes from the centre to the periphery of most of the cells. This is because of differences in thickness at the centre and towards the edges, so there are more chromophores in the centre than at the edges.

INDO's emission properties at 405 nm and 480 nm change upon binding to  $\text{Ca}^{2+}$  ( $\lambda_{\text{exc}} = 350$  nm). The two emission intensities can easily be measured by using a beam splitter, two interference filters and two photomultipliers; it is fairly difficult to envisage the use of two intensified cameras to form an image unless one uses a specifically split CCD array. Therefore INDO has been applied in processes that require either rapid determination of the free calcium concentration (i.e. cell sorting), or where the kinetics of the free calcium change are fast.

Fura-2, upon binding to calcium, undergoes a change in its absorption spectrum and therefore in its excitation spectrum; namely the emission intensity (collected at  $\lambda_{\text{em}} = 510$  nm and higher) increases at  $\lambda_{\text{exc}} = 340$  nm and decreases at  $\lambda_{\text{exc}} = 380$  nm (**Figure A5.6**). A typical property of all the indicators that undergo either an excitation or emission shift is the presence of an 'isosbestic point', namely the presence of a 'unique point' in the spectrum when the parameter concentration is changed ( $\text{Ca}^{2+}$  in the case of Fura-2). The isosbestic point is only present when two species are in equilibrium (in our case calcium-bound and free forms of Fura-2 or of INDO). The

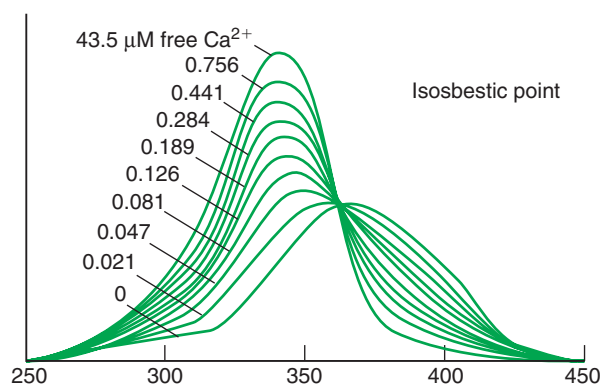


**FIGURE A5.6** Excitation spectral changes of Fura-2 as a function of  $\text{Ca}^{2+}$  concentration.

Each curve represents the intensity of fluorescence emitted by Fura-2 (at  $\lambda = 510$  nm) as a function of the wavelength of excitation (from 250 to 450 nm) and for a given  $\text{Ca}^{2+}$  concentration (from 0 to 43.5  $\mu\text{M}$ ). Knowing that  $\text{Fura-2} + \text{Ca}^{2+} \rightleftharpoons \text{Fura-2-Ca}$ , the curve obtained in the presence of the maximal  $\text{Ca}^{2+}$  concentration (43.5  $\mu\text{M}$ ) represents the excitation spectrum of the bound form of Fura (Fura-2-Ca). In contrast, the curve obtained for the minimal  $\text{Ca}^{2+}$  concentration (0  $\mu\text{M}$ ) represents the excitation spectrum of the free form of Fura (Fura-2). It appears clearly that measured at  $\lambda = 340/350$  nm and at  $\lambda = 380$  nm, the intensity of fluorescence emitted by Fura-2 varies with the ratio free/bound forms of Fura; i.e., with  $\text{Ca}^{2+}$  concentration.

absence of this point can be taken as an indicator for the contamination by an other ion. This point appears at 360 nm for Fura-2 (**Figure A5.6**). As Fura-2 undergoes a change in its absorption properties, alternating the excitation filters at the two chosen wavelengths, mostly at 340 and 380 nm, and collecting the emission above 510 nm with an intensified camera, one can construct the free calcium image, or the time series of the changing free  $\text{Ca}^{2+}$  concentration in a living cell, by calculating the free  $\text{Ca}^{2+}$  concentration at each pixel (picture element). One is not limited to these two wavelengths; it might even be advantageous to take the images at longer wavelengths than 340 nm as most of the optical path of old fluorescence microscopes is opaque to this wavelength.

With the advent of confocal microscopy, an indicator with absorption properties in the visible part of the spectrum was needed (confocal microscopes use laser scanning, and ultraviolet lasers have been recently developed but are still too expensive). FLUO-3, Calcium Green and Oregon Green were developed to respond to this need. The main disadvantage of these probes is that their quantum efficiency changes at one wavelength only ( $\sim 530$  nm, when excited at the 488 nm line of the argon laser) upon binding to  $\text{Ca}^{2+}$  ions. It is therefore not possible to measure absolute values of  $\text{Ca}^{2+}$  concentrations directly; nevertheless, if the resting level of the free  $\text{Ca}^{2+}$  concentration in the cell is known, the values obtained before stimulation can be used to calculate the

approximate value of the free  $\text{Ca}^{2+}$  concentration under stimulation.

Experience shows that fluorescence intensity always seems too low, and it is tempting to increase the concentration of the reporter molecule inside the cell to overcome this problem. In the case of  $\text{Ca}^{2+}$  measurements this will have the adverse effect of buffering free  $\text{Ca}^{2+}$  ions and to prevent its rise (BAPTA-like backbone). It is necessary to find a compromise between the signal-to-noise level and the buffering of the ion in general, the best approach being the use of the least amount of indicator required for the job.

#### Indicators for $\text{Mg}^{2+}$ and other divalents

Mag-Fura and Magnesium Green are  $\text{Mg}^{2+}$  indicators. They are designed around the same EGTA chelator structure as for  $\text{Ca}^{2+}$  indicators.  $\text{Mg}^{2+}$  indicators are designed to respond maximally to the  $\text{Mg}^{2+}$  concentrations commonly found in cells – typically 0.1–6 mM. They also bind  $\text{Ca}^{2+}$  with a low affinity. Typical physiological  $\text{Ca}^{2+}$  concentrations (10 nM–1  $\mu\text{M}$ ) do not usually interfere with  $\text{Mg}^{2+}$  measurements. Although  $\text{Ca}^{2+}$  binding to  $\text{Mg}^{2+}$  indicators can be a complicating factor in  $\text{Mg}^{2+}$  measurements, this property can also be exploited for measuring high  $\text{Ca}^{2+}$  concentrations (1–100  $\mu\text{M}$ ) such as those seen in the mitochondria. Mag-Fura and Magnesium Green do have similar spectral properties as their calcium counterparts.

Most of the reporter molecules synthesized for  $\text{Ca}^{2+}$  or  $\text{Mg}^{2+}$  also interact with other polyvalent ions such as  $\text{Tb}^{3+}$ ,  $\text{Cd}^{2+}$ ,  $\text{Hg}^{2+}$ ,  $\text{Ni}^{2+}$  and  $\text{Ba}^{2+}$ , and in some cases with better quantum yields. This annoying property can be turned into advantage, when one wants to measure changes in the concentrations of those ions.

#### Indicators for $\text{Na}^+$ and $\text{K}^+$

SBFI and PBF1 are designed around a crown ether chelator to which benzofuranyl chromophores are linked, conferring to those molecules the same spectroscopic properties as Fura. Hence the same filter sets can be used as for Fura. The cavity size of the crown ether is the factor which determines the specificity of the molecule for  $\text{Na}^+$  or  $\text{K}^+$ . The specificities of both SBFI and PBF1 for their respective ions is much smaller than that of Fura for  $\text{Ca}^{2+}$ , and the  $K_D$  changes as a function of the concentration of the other ion, the ionic strength, pH and temperature.

Sodium Green is designed around a crown ether chelator to which two dichlorofluorescein chromophores are linked, resulting in similar spectroscopic properties as Calcium Green (i.e. excited at 488 nm). The cavity size of the crown ether results in a greater selectivity for  $\text{Na}^+$  over  $\text{K}^+$  compared with SBFI – 41 versus

18 times, respectively. The spectral properties, however, result in emission changes at one wavelength only, so ratiometric measurements with this reporter molecule are not possible.

All of the cation reporter molecules suffer  $K_D$  changes as a result of intracellular interactions as mentioned above, so they need to be calibrated *in situ* using pore-forming antibiotics like gramicidin and loading the cells with known ionic conditions. Another point which must be borne in mind is the fact that protein dye interactions might dampen or completely eliminate the signals.

#### Indicators for $\text{Cl}^-$

All of the chloride indicators are based on methoxyquinolinium derivatives and report the chloride by the diffusion-limited collisional quenching of the chromophore in the excited state interacting with the halide ion. The quenching is not accompanied by spectral shifts, so ratiometric measurements are not possible. As the quenching depends on collisional encounters of the halide ion, it is very sensitive to intracellular viscosity and temperature. The quenching efficiency is greater for the other halides such as  $\text{Br}^-$  and  $\text{I}^-$ .

#### Voltage-sensitive dyes

Voltage-sensitive dyes enable us to measure membrane potential in cells or organelles that are too small for microelectrode impalement. Moreover, these probes can map variations of membrane potential with spatial resolution and sampling frequency that are difficult to achieve using microelectrodes, such as cells microdomains or full network studies. Potentiometric probes include many chemical structures (styryl, carbocyanines and rhodamines, oxonols derived ... as examples), the existence of numerous dyes analogs reflects the observation that no single dye provides the optimal response under all experimental conditions. Selecting the best voltage-sensitive probe might be empirical and the choice of the class of dye is determined by different factors such as accumulation in cells, response mechanisms, toxicity or kinetics of the electrical events observed. Voltage-sensitive dyes are divided into two categories concerning this last parameter: (i) fast-response probes that are sufficiently fast to detect transient (millisecond) potential changes in excitable cells. However, the magnitude of their potential-dependent fluorescence change is often small; they typically show a 2–10% fluorescence change per 100 mV; (ii) slow-response probes; the magnitude of their optical responses is much larger than that of fast-response probes (typically a 1% fluorescence change per mV). Slow-response probes are suitable for detecting changes in average membrane potentials of non-excitable cells caused by respiratory activity, ion-channel permeability, drug binding and other factors.

## FURTHER READING

Denk W, Strickler JH, Webb WW (1990) Two-photon laser scanning fluorescence microscopy. *Science* **248**, 73–76.

Tsien RY (1989) Fluorescent probes of cell signaling. *Annu. Rev. Neurosci.* **12**, 227–253.

<http://www.molecularexpressions.com/primer/techniques/fluorescence/filters.html>

<http://www.molecularexpressions.com/index.html>

<http://probes.invitrogen.com/handbook/>

## APPENDIX 5.2 TAIL CURRENTS

Tail currents are observed in voltage or patch clamp experiments. ‘Tail’ means that the voltage-gated current is observed at the end of a depolarizing voltage step, upon sudden removal of the depolarization of the membrane. Tail currents do not exist in physiological conditions; they are ‘experimental artifacts’. However, there are several reasons for studying tail currents: they are tools for determining characteristics of currents such as reversal potential and inactivation rate constants. Tail currents were first described by Hodgkin and Huxley (1952) in the squid giant axon.

### Single-channel tail current

In patch clamp recordings of the activity of a single voltage-gated channel, a unitary current of much larger amplitude is occasionally observed at the end of the voltage step (Figure A5.7). It corresponds to the current flowing through a channel that is not yet closed at the end of the depolarizing step. Therefore tail currents are recorded for voltage-gated channels that do not rapidly close or inactivate during a depolarizing step, such as delayed rectifier  $K^+$  or L-type  $Ca^{2+}$  channels.

The activity of an L-type  $Ca^{2+}$  channel is recorded in patch clamp (cell-attached patch) in the presence of the selective agonist Bay K 8644. On stepping back the membrane to the holding potential, the L-type  $Ca^{2+}$  channel opened by the preceding depolarization does

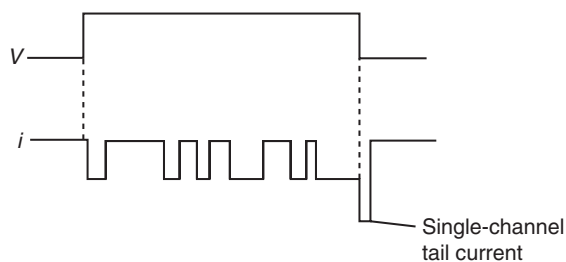


**FIGURE A5.7** Activity of an L-type  $Ca^{2+}$  channel. Recorded in patch clamp (cell-attached patch) in the presence of 110 mM external  $Ba^{2+}$ . In response to a depolarizing step in the presence of 5  $\mu$ M Bay K 8644, a single-channel current of larger amplitude is recorded upon repolarization. It is a single-channel  $Ca^{2+}$  tail current.

not immediately close since the transition  $O \rightleftharpoons C$  is not immediate. The inward unitary  $Ca^{2+}$  current recorded at this moment is larger (Figure A5.7) because of the larger driving force upon removal of depolarization than during the depolarizing step: during the depolarizing step to 0 mV,  $i_{Ca} = \gamma_{Ca} (V_m - E_{Ca}) = \gamma_{Ca} (0 - 50) = -50\gamma_{Ca}$ ; upon removal of depolarization  $i_{Ca} = \gamma_{Ca} (V_m - E_{Ca}) = \gamma_{Ca} (-60 - 50) = -110\gamma_{Ca}$ .

Then, after a few milliseconds, owing to closing of the channel, the tail current returns to zero (the voltage-gated channel closes in response to the repolarization of the membrane).

### Whole-cell tail current

In voltage or whole-cell patch clamp recordings (in the presence of  $Na^+$  and  $K^+$  channel blockers), a voltage step to 0 mV from a holding potential of  $-40$  mV activates a number  $N$  of L-type  $Ca^{2+}$  current is recorded. At the end of the voltage step a  $Ca^{2+}$  current of larger amplitude and small duration is always recorded: the tail  $Ca^{2+}$  current (Figure A5.8). Then the amplitude of this tail current progressively diminishes. The peak of the whole-cell tail current has a larger

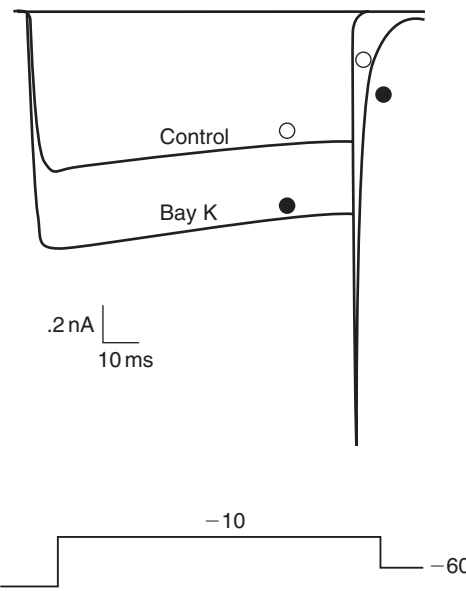


**FIGURE A5.8** Activity of a dorsal root ganglion neuron. Recorder in single-electrode voltage clamp in the presence of  $Na^+$  and  $K^+$  channel blockers and 2 mM external  $Ba^{2+}$ . A depolarization to  $-10$  mV followed by a repolarization to  $-60$  mV is applied to the membrane from a holding potential  $V_H = -90$  mV. The depolarizing step evokes an inward  $Ba^{2+}$  current followed by an inward  $Ba^{2+}$  tail current (control, open circle). The presence of 1  $\mu$ M Bay K 8644 increases the amplitude of the  $Ba^{2+}$  current during the step. It also prolongs the  $Ba^{2+}$  tail current (black circle). Adapted from Carbone E, Formenti A, Pollo A (1990) Multiple actions of Bay K 8644 on high-threshold Ca channels in adult rat sensory neurons. *Neurosci. Lett.* **111**, 315–320, with permission.

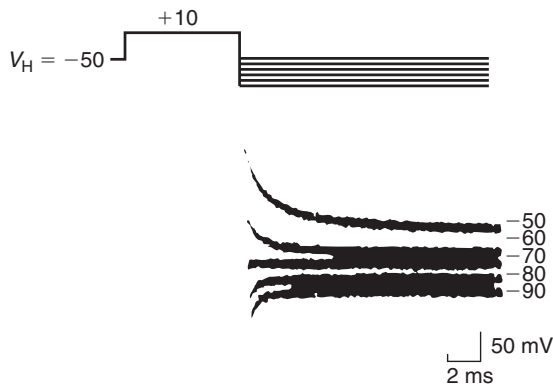


**FIGURE A5.9** Activity of a chick dorsal root ganglion cell. Recorded in single-electrode voltage clamp, in the presence of  $1 \mu\text{M}$  TTX and  $10 \text{ mM CO}_2^{+}$  to block, respectively,  $\text{Ca}^{2+}$  and  $\text{Na}^{+}$  channels. Depolarizations to  $+10 \text{ mV}$  from a holding potential of  $-50 \text{ mV}$  followed by successive repolarizations to  $-50$ ,  $-60$ ,  $-70$ ,  $-80$  and  $-90 \text{ mV}$  are applied ( $V$  traces). Bottom  $I$  traces show the  $\text{K}^{+}$  tail currents at the corresponding membrane potentials (the outward  $\text{K}^{+}$  current during the step is not shown). The reversal potential of the  $\text{K}^{+}$  tail current is  $-70 \text{ mV}$ . It indicates the value of  $E_{\text{K}}$  in these cells. To separate the ionic tail current from the capacitive current, the latter was subtracted from the total current by digital summation of the currents elicited with identical depolarizing and hyperpolarizing test pulses. Adapted from Dunlap K, Fischbach GD (1981) Neurotransmitters decrease the calcium conductance activated by depolarization of embryonic chick sensory neurones. *J. Physiol.* **317**, 519–535, with permission.

amplitude than that of the whole-cell current recorded during the voltage step since the driving force for  $\text{Ca}^{2+}$  ions is larger upon removal of depolarization than during the depolarization, as explained above.

The tail current diminishes progressively owing to the progressive closure of the  $N$  open  $\text{Ca}^{2+}$  channels: the channels do not all close at the same time once the membrane is repolarized. The whole-cell tail current of **Figure A5.8** represents the summation of hundreds to thousands of recordings of single-channel tail currents.

In **Figures A5.7** and **A5.8**, the tail currents are inward. The direction of a tail current (as for any type of current) depends on the sign of the driving force; i.e. the value of membrane potential upon repolarization ( $V_{\text{H}}$ ) and that of the reversal potential of the current ( $E_{\text{rev}}$ ) which depends on the ions flowing through the open channels. By varying the voltage at the end of the depolarizing step the tail current varies in amplitude and direction (inward to outward or the reverse) and it is possible to determine the reversal potential of the tail current under study: when  $V_{\text{H}} = E_{\text{rev}}$  the tail current is equal to zero (**Figure A5.9**). This values of  $E_{\text{rev}}$  is the same for the tail

current and the current recorded during the voltage step since it concerns the same channels.

The voltage protocol of **Figure A5.9** allows the determination of  $E_{\text{rev}}$  and consequently identification of the type of ions that carry the current  $E_{\text{rev}}$  can also be determined directly by changing the voltage-step value. However, for  $\text{K}^{+}$  channels for example,  $E_{\text{rev}}$  is near  $-100 \text{ mV}$ , a membrane potential where the open probability of voltage-gated channels is very low. By using tail currents, this problem is overcome.

## FURTHER READING

- Bertolino M and Llinas RR (1992) The central role of voltage-activated and receptor-operated calcium channels in neuronal cells. *Ann. Rev. Pharmacol. Toxicol.* **32**, 399–421.
- Caterall WA (1998) Structure and function of neuronal  $\text{Ca}^{2+}$  channels and their role in transmitter release. *Cell Calcium* **24**, 307–323.
- De Leon M, Wang Y, Jones J *et al.* (1995) Essential  $\text{CA}^{2+}$ -binding motif for  $\text{Ca}^{2+}$ -sensitive inactivation of L-type  $\text{CA}^{2+}$  channels. *Science* **270**, 1502–1506.
- Denk W, Piston DW, Webb WW (1995) Two-Photon molecular excitation in laser-scanning microscopy. In Pawley JB (ed.) *Handbook of Biological Microscopy*. New York: Plenum Press.
- Felix R (1999) Voltage-dependent  $\text{Ca}^{2+}$  channel  $\alpha_2$ -delta auxiliary subunit: structure, function and regulation. *Recept. Chann.* **6**, 351–362.
- Grynkievicz G, Poenie M, Tsien RY (1985) A new generation of calcium indicators with greatly improved fluorescence properties. *J. Biol. Chem.* **260**, 3440–3448.
- Hodgkin AL and Huxley AF (1952) A quantitative description of membrane current and its application to conduction and excitation in nerve. *J. Physiol. (Lond.)* **117**, 500–544.
- Hofmann F, Lacinova L, Klugbauer N (1999) Voltage-dependent calcium channels: from structure to function. *Rev. Physiol. Biochem. Pharmacol.* **139**, 33–87.
- Miller C (1995) The charybdotoxin family of  $\text{K}^{+}$  channel-blocking peptides. *Neurons* **15**, 5–10.
- Neher E and Augustine GJ (1992) Calcium gradients and buffers in bovine chromaffin cells. *J. Physiol. (Lond.)* **450**, 273–301.
- Randall A and Benham CD (1999) Recent advances in the molecular understanding of voltage-gated  $\text{Ca}^{2+}$  channels. *Cell Neurosci.* **14**, 255–272.
- Stein A, Soong TW, Snutch TP (1995) Determinants of PKC-dependent modulation of a family of neuronal calcium channels. *Neuron* **15**, 929–940.
- Tan YP, Llano I, Hopt A, Wuerrlihausen F, Neher E (1999) Fast scanning and efficient photodetection in a simple two-photon microscope. *J. Neurosci. Meth.* **92**, 123–135.
- Tsien RY (1989) Fluorescent probes of cell signalling. *Ann. Rev. Neurobiol.* **12**, 221–253.
- Varadi G, Mori Y, Mikala G, Schwartz A (1995) Molecular determinants of  $\text{Ca}^{2+}$  channels function and drug action. *Trend. Pharmacol. Sci.* **16**, 43–49.
- Zamponi GW, Bourinet E, Nelson D, Nargeot J, Snutch TP (1997) Crosstalk between G proteins and protein kinase C mediated by the calcium channel  $\alpha_1$  subunit. *Nature* **385**, 442–446.